Resource

Cell

A White-Box Machine Learning Approach for Revealing Antibiotic Mechanisms of Action

Graphical Abstract

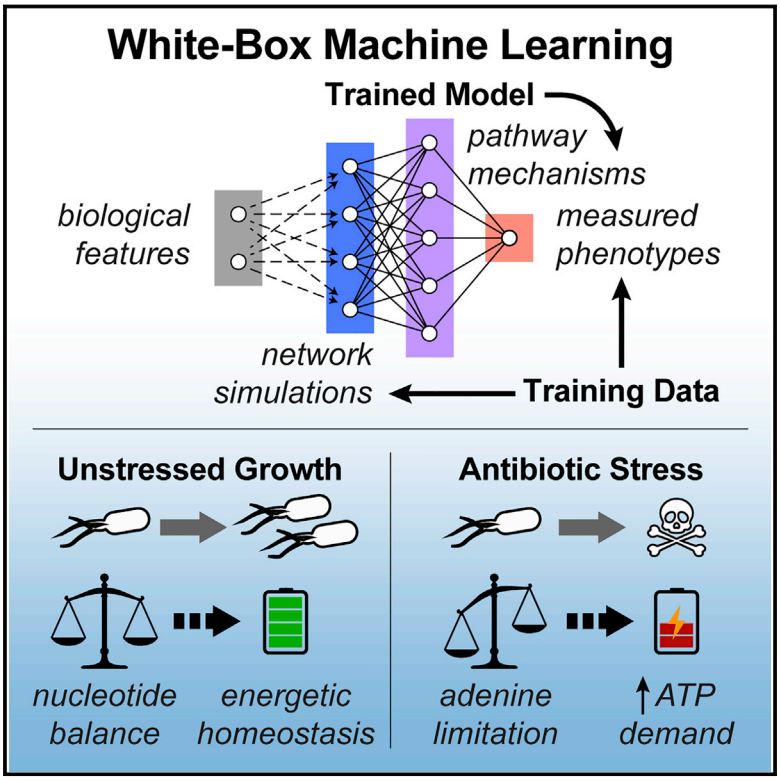

Authors

Jason H. Yang, Sarah N. Wright, Meagan Hamblin, ..., Bernhard O. Palsson, Graham C. Walker, James J. Collins

Correspondence

jimjc@mit.edu

In Brief

Causal metabolic pathways underlying antibiotic lethality in bacteria are illuminated by a network model-driven machine learning approach, overcoming limitations of existing “black-box” approaches that cannot reveal causal relationships from large biological datasets.

Highlights

- A white-box machine learning approach is developed for antibiotics research
- Network modeling is coupled to a biochemical screen to identify pathway mechanisms
- Antibiotic-induced adenine limitation increases purine biosynthesis and ATP demand
- Increased ATP demand drives central carbon metabolism and oxygen consumption

Yang et al., 2019, Cell *177*, 1649–1661
May 30, 2019
https://doi.org/10.1016/j.cell.2019.04.016

CellPress

Resource

Cell

A White-Box Machine Learning Approach for Revealing Antibiotic Mechanisms of Action

Jason H. Yang,[1,2] Sarah N. Wright,[1,2,8] Meagan Hamblin,[2,8] Douglas McCloskey,[3] Miguel A. Alcantar,[1,2] Lars Schrübbers,[3] Allison J. Lopatkin,[1,2,4] Sangeeta Satish,[5] Amir Nili,[5] Bernhard O. Palsson,[3,6] Graham C. Walker,[7] and James J. Collins[1,2,4,9,*]

[1]Institute for Medical Engineering and Science and Department of Biological Engineering, Massachusetts Institute of Technology, Cambridge, MA 02139, USA
[2]Infectious Disease and Microbiome Program, Broad Institute of MIT and Harvard, Cambridge, MA 02142, USA
[3]Novo Nordisk Foundation Center for Biosustainability, Technical University of Denmark, 2800 Lyngby, Denmark
[4]Wyss Institute for Biologically Inspired Engineering, Harvard University, Boston, MA 02115, USA
[5]Department of Biomedical Engineering, Boston University, Boston, MA 02215, USA
[6]Department of Bioengineering, University of California, San Diego, La Jolla, CA 92093, USA
[7]Department of Biology, Massachusetts Institute of Technology, Cambridge, MA 02139, USA
[8]These authors contributed equally
[9]Lead Contact
*Correspondence: jimjc@mit.edu
https://doi.org/10.1016/j.cell.2019.04.016

SUMMARY

Current machine learning techniques enable robust association of biological signals with measured phenotypes, but these approaches are incapable of identifying causal relationships. Here, we develop an integrated "white-box" biochemical screening, network modeling, and machine learning approach for revealing causal mechanisms and apply this approach to understanding antibiotic efficacy. We counter-screen diverse metabolites against bactericidal antibiotics in *Escherichia coli* and simulate their corresponding metabolic states using a genome-scale metabolic network model. Regression of the measured screening data on model simulations reveals that purine biosynthesis participates in antibiotic lethality, which we validate experimentally. We show that antibiotic-induced adenine limitation increases ATP demand, which elevates central carbon metabolism activity and oxygen consumption, enhancing the killing effects of antibiotics. This work demonstrates how prospective network modeling can couple with machine learning to identify complex causal mechanisms underlying drug efficacy.

INTRODUCTION

Recent advances in high-throughput experimental technologies and data analyses have enabled unprecedented observation, quantification, and association of biological signals with cellular phenotypes. Data-driven machine learning activities are poised to transform biological discovery and the treatment of human disease (Camacho et al., 2018; Wainberg et al., 2018; Webb, 2018; Yu et al., 2018a); however, existing techniques for extracting biological information from large datasets frequently encode relationships between perturbation and phenotype in opaque "black-boxes" that are mechanistically uninterpretable and, consequently, can only identify correlative as opposed to causal relationships (Ching et al., 2018). In natural systems, biological molecules are biochemically organized in networks of complex interactions underlying observable phenotypes; biological network models may therefore harbor the potential to provide mechanistic structure to machine learning activities, yielding transparent "white-box" causal insights (Camacho et al., 2018; Yu et al., 2018b).

Chemical and genetic screens are workhorses in modern drug discovery but frequently suffer from poor (1%–3%) hit rates (Roses, 2008). Such low hit rates often underpower the bioinformatic analyses used for causal inference because of limitations in biological information content. Experimentally validated network models possess the potential to expand the biological information content of sparse screening data; however, biological screening experiments are typically performed independently from network modeling activities, limiting subsequent analyses to either *post hoc* bioinformatic enrichment from screening hits or experimental validation of existing models. Therefore, there is a need to develop biological discovery approaches that integrate biochemical screens with network modeling and advanced data analysis techniques to enhance our understanding of complex drug mechanisms (Camacho et al., 2018; Wainberg et al., 2018; Xie et al., 2017). Here we develop one such approach and apply it to understanding antibiotic mechanisms of action.

Antibiotics, a cornerstone of modern medicine, are threatened by the increasing burden of drug resistance, which is compounded by a diminished antimicrobial discovery pipeline (Brown and Wright, 2016). Although the primary targets and mechanisms of action for conventional antibiotics are well studied (Kohanski et al., 2010), there is growing appreciation that secondary processes, such as altered metabolism, actively participate in antibiotic efficacy (Yang et al., 2017a) and that

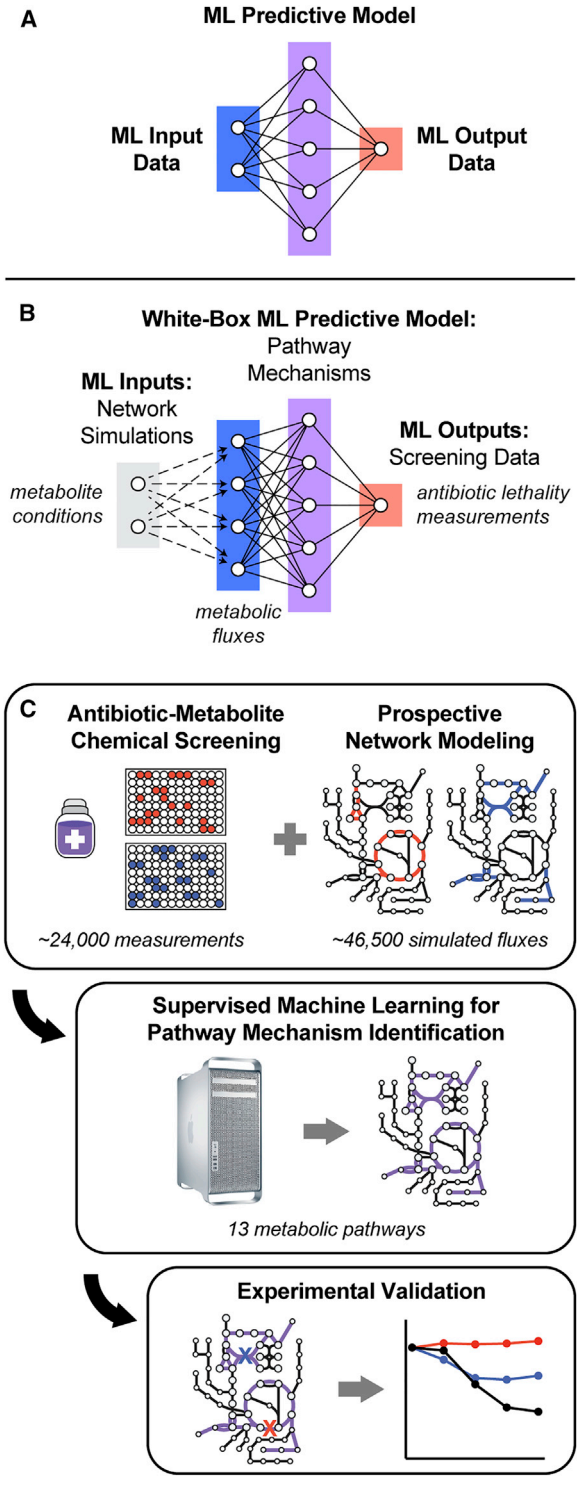

Figure 1. A White-Box Machine Learning Approach for Revealing Metabolic Mechanisms of Antibiotic Lethality

(A) Machine learning activities are typically comprised of three parts: input data (blue), output data (red), and a predictive model trained to compute output data from input data (purple).

(B) An overall framework for white-box machine learning. Input screening perturbations (e.g., metabolite conditions; gray) are first transformed into enriched biological network states by prospective network modeling (e.g., metabolic fluxes; blue). These network simulations are then used as machine learning inputs to train a predictive model (purple), revealing pathway mechanisms underlying the output data (e.g., antibiotic lethality measurements; red). Because biological networks are mechanistically constructed, features comprising the predictive models trained by machine learning are, by definition, mechanistically causal.

(C) *E. coli* MG1655 cells were treated with three bactericidal antibiotics at 13 or more different concentrations. Antibiotic IC_{50} values were quantified following supplementation with 206 diverse metabolites and normalized by their on-plate controls. Metabolic network states corresponding to each metabolite were prospectively simulated using the iJO1366 model of *E. coli* metabolism (Orth et al., 2011). For each antibiotic, changes in IC_{50} were regressed on the simulated fluxes, and pathway mechanisms were identified by hypergeometric testing on metabolic pathways curated by Ecocyc (Keseler et al., 2017). Identified pathways were validated experimentally.

extracellular metabolites may either potentiate (Allison et al., 2011; Meylan et al., 2017) or suppress (Yang et al., 2017b) the lethal activities of bactericidal antibiotics. Although features of central metabolism (Kohanski et al., 2007) and cellular respiration (Gutierrez et al., 2017; Lobritz et al., 2015) are implicated in antibiotic lethality across diverse microbial species (Dwyer et al., 2015), the biological mechanisms underlying antibiotic-induced changes to metabolism (Belenky et al., 2015; Dwyer et al., 2014) remain unclear. A deeper understanding of how bacterial metabolism interfaces with antibiotic lethality has the potential to open new drug discovery paradigms (Bald et al., 2017; Murima et al., 2014), making antibiotic-induced cellular death physiology an attractive topic to investigate with white-box machine learning.

Here, we integrate biochemical screening, network modeling, and machine learning to form a white-box machine learning approach to reveal drug mechanisms of action. We apply this approach to elucidating metabolic mechanisms of action for bactericidal antibiotics. We discover that metabolic processes related to purine biosynthesis, driven by antibiotic-induced adenine limitation, participate in antibiotic lethality. We show that adenine limitation increases ATP demand via purine biosynthesis, resulting in elevated central carbon metabolism activity and oxygen consumption, thereby enhancing the killing effects of antibiotics. This work demonstrates how network models can facilitate machine learning activities for biological discovery and provide insights into the complex causal mechanisms underlying drug efficacy.

RESULTS

A White-Box Machine Learning Approach for Revealing Metabolic Mechanisms of Antibiotic Lethality

Machine learning aims to generate predictive models from sets of training data; such activities are typically comprised of three parts: input data, output data, and the predictive model trained to compute output data from input data (Figure 1A; Camacho et al., 2018). Although modern machine learning methods can assemble high-fidelity input-output associations from training data, the functions comprising the resulting trained models often do not possess tangible biochemical analogs, rendering them mechanistically uninterpretable. Consequently, predictive

models generated by such (black-box) machine learning activities are unable to provide direct mechanistic insights into how biological molecules are interacting to give rise to observed phenomena. To address this limitation, we developed a white-box machine learning approach, leveraging carefully curated biological network models to mechanistically link input and output data (Yu et al., 2018b).

Our approach integrates biochemical screening with prospective network modeling to provide mechanistically linked training data for machine learning (Figure 1B). In contrast to existing data-driven approaches, which generate predictive models from only the variables or perturbations available in a screen, we first use prospective network modeling to quantitatively transform screening perturbations into biologically enriched network states. Biological information from experimental screens are applied as boundary conditions to the network simulations, computing a network representation for each perturbation in the screen (e.g., metabolic fluxes following metabolite perturbations). These network representations are then used as input data to train predictive models with the empirical screening measurements (e.g., quantified cellular phenotypes in response to screening perturbations) as output data. Because biological networks are mechanistically constructed, the features comprising the predictive models trained by machine learning are, by definition, mechanistically causal and represent tangible biochemical species that can be directly tested experimentally.

Here we applied this integrated screening-modeling-learning approach to investigate metabolic mechanisms of antibiotic lethality, demonstrating the ability of this workflow to reveal new mechanistic insights (Figure 1C). Specifically, we designed biochemical screens to measure the effects of diverse metabolite supplementations on the lethality of three bactericidal antibiotics: ampicillin (AMP, a β-lactam), ciprofloxacin (CIP, a fluoroquinolone), and gentamicin (GENT, an aminoglycoside). We screened combinations of these antibiotics and metabolites in *Escherichia coli*, measuring their antibiotic half-maximal inhibitory concentrations (IC_{50}) after 4 h of treatment. Next we prospectively simulated metabolic network states corresponding to each metabolite perturbation using the iJO1366 genome-scale model of *E. coli* metabolism (Orth et al., 2011) with quantitative information from the biochemical screens as modeling constraints. These simulations comprehensively yield flux estimates for each metabolic reaction in *E. coli* under each screening condition. For each antibiotic, we applied machine learning regression analyses to train a predictive model that could reveal pathway mechanisms underlying differences in antibiotic lethality measured in our screen. These pathways were identified by regularizing the simulated metabolic network states, regressing the measured IC_{50} values, and performing enrichment analyses from metabolic pathway annotations curated in Ecocyc v.22.0 (Keseler et al., 2017).

Exogenous Metabolites Exert Pathway-Specific Effects on Antibiotic Lethality

Input-output relationships between *E. coli* metabolism and antibiotic lethality were systematically quantified by measuring antibiotic IC_{50} values following supplementation with metabolites known to participate in *E. coli* metabolism (Figure 2A). To avoid the potentially confounding effects of stationary-phase physiology on antibiotic tolerance, we performed experiments using exponentially growing *E. coli* MG1655 cells. These cells were grown in 3-(*N*-morpholino)propanesulfonate (MOPS)-defined minimal medium (Neidhardt et al., 1974) and systematically screened with an unbiased and semi-comprehensive library of metabolites against AMP, CIP, and GENT. Screened metabolites were derived from the Biolog phenotype microarrays (PMs) 1–4 (Bochner, 2009), which are comprised of diverse carbon, nitrogen, phosphorus, and sulfur species. These PMs contain 206 unique amino acids, carbohydrates, nucleotides, and organic acids that are included in the iJO1366 genome-scale model of *E. coli* metabolism. Antibiotic responses to these 206 metabolites were used for subsequent analyses (Table S1).

Changes in antibiotic IC_{50} values were modest; in most cases, less than 2-fold (Figure 2B; Table S2). Hierarchical clustering of the measured IC_{50} values revealed that the metabolite response profiles differed between AMP, CIP, and GENT, highlighting their different biochemical targets. However, several metabolites appeared to commonly potentiate or inhibit efficacy across multiple antibiotics, indicating shared metabolic mechanisms of action. Interestingly, many nitrogen, phosphorus, and sulfur metabolites increased antibiotic IC_{50} values, whereas many carbon metabolites decreased IC_{50} values, similar to previous observations (Yang et al., 2017b). These raw data indicate that the measured antibiotic lethality responses to metabolite perturbations occurred through specific metabolic pathways rather than generically as a response to medium enrichment.

Conventional Bioinformatic Analyses Do Not Provide Novel Mechanistic Insights

To test the capabilities of conventional bioinformatic analyses to yield mechanistic insights into how the screened metabolites alter antibiotic lethality, we first performed an enrichment analysis of metabolites that elicited a 2-fold or more change in IC_{50}, a conventional definition for a screening "hit" (Table S3). For each antibiotic, a metabolite set enrichment analysis was performed in Ecocyc. For AMP (2 metabolites $\geq$ 2-fold change in IC_{50}) and GENT (8 metabolites $\geq$ 2-fold change in IC_{50}), no pathways were enriched with less than a 5% false discovery rate (FDR) ($q \leq 0.05$). For CIP (19 metabolites $\geq$ 2-fold change in IC_{50}), several non-specific pathways related to protein translation were identified, with top enrichments including "aminoacyl-tRNA charging" ($p = 1.98e{-}6$), "proteinogenic amino acid biosynthesis" ($p = 2.50e{-}6$), and "amino acid degradation" ($p = 1.27e{-}5$) (Table S4). These findings are consistent with previous observations that protein translation inhibitors generally exert antagonistic effects on antibiotic lethality (Lobritz et al., 2015; Ocampo et al., 2014). Collectively, these results illustrate two common weaknesses in conventional bioinformatic approaches for analyzing biochemical screens: statistical power limitations and low-specificity associations.

White-Box Machine Learning Reveals Known and New Antibiotic Mechanisms of Action

We next applied our white-box machine learning approach and prospectively modeled metabolic network states corresponding

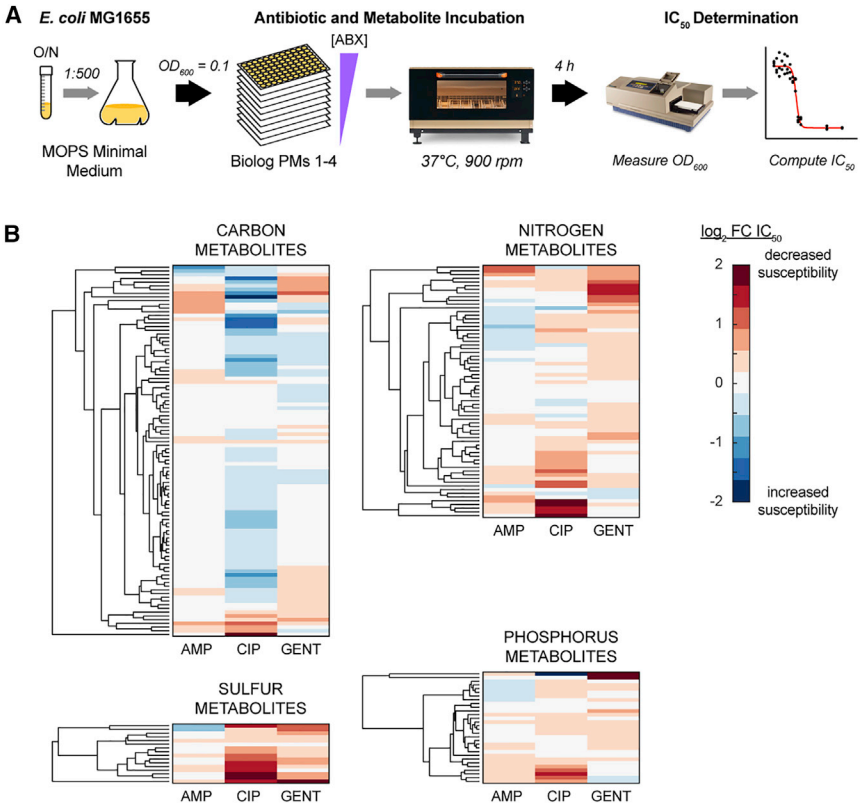

Figure 2. Exogenous Metabolites Exert Pathway-Specific Effects on Antibiotic Lethality

(A) Overall experimental design for measuring metabolite effects on antibiotic lethality. Overnight cultures of *E. coli* MG1655 were inoculated into MOPS minimal medium, grown to early exponential phase, and back-diluted to OD_{600} = 0.1. Cells were dispensed into Biolog phenotype microarray (PM) plates 1–4 (Bochner, 2009) with different concentrations of ampicillin (AMP), ciprofloxacin (CIP), or gentamicin (GENT) added. OD_{600} was measured after 4 h of incubation at 37°C and shaking at 900 rpm. Antibiotic IC_{50} values were estimated for each antibiotic-metabolite combination.

(B) Antibiotic IC_{50} responses to metabolite supplementation. Metabolically induced sensitivity profiles differ by antibiotic, but several metabolites commonly protect (red) or sensitize (blue) cells to multiple antibiotics. Carbon metabolites were screened using Biolog PMs 1 and 2, nitrogen metabolites were screened using Biolog PM 3, and phosphorus and sulfur metabolites were screened using Biolog PM 4.

Data are represented as mean from n ≥ 3 independent biological replicates.

to supplementation with each metabolite used in the screen. For each metabolite, metabolic states were simulated by first adding exchange reactions to the *E. coli* metabolic model, which enabled uptake of each metabolite from the extracellular environment. We then performed parsimonious flux balance analysis (pFBA) (Lewis et al., 2010) under conditions simulating MOPS minimal medium and optimized for the biomass objective function (Table S5). Although this approach does not explicitly model contributions by gene expression toward changes in metabolism, benchmarking studies demonstrate that principles of growth maximization and parsimony are sufficient for accurately predicting metabolism in defined metabolic environments (Machado and Herrgård, 2014).

For each antibiotic, metabolic pathway mechanisms were identified by first conducting a dimension-reducing machine learning regression task and then performing hypergeometric statistical testing on metabolic reactions comprising the resulting predictive model using pathway-reaction sets curated by Ecocyc. The measured changes in antibiotic IC_{50} were jointly learned on the set of simulated metabolic network states using a multitask elastic net (Caruana, 1997; Zou and Hastie, 2005), yielding 477 reactions predicted to alter antibiotic lethality. For each antibiotic, reactions with coefficients whose magnitude were less than or equal to half the SD of all coefficients were removed to exclude spurious reactions selected by joint learning. For AMP, CIP, and GENT, this yielded 189, 208, and 204 reactions, respectively (Table S6). Next, hypergeometric statistics were performed on Ecocyc-curated pathways. Of the 431 metabolic pathways curated by Ecocyc, only 13 were found to be statistically significant, with less than a 5% FDR for at least one antibiotic (Table S7).

Because our white-box machine learning approach yields pathway mechanisms, we can quantify the relative contributions of each metabolic pathway to the lethal mechanisms of each antibiotic. We computed pathway scores for each pathway and antibiotic by performing least-squares regression on the changes in antibiotic IC_{50} and then log-transforming the average non-zero regression coefficients for all reactions in each pathway. Identified pathways primarily clustered into three groups based on their pathway scores (Figure 3). One cluster possessed central carbon metabolism pathways (“superpathway of glycolysis, pyruvate dehydrogenase, tricarboxylic acid [TCA], and glyoxylate bypass”; “superpathway of glyoxylate bypass and TCA”; and “TCA cycle I (prokaryotic)”) with similar pathway directionality for AMP, CIP, and GENT (indicated by the sign of the pathway score). These findings are consistent with several studies demonstrating the TCA cycle to be a shared mechanism in antibiotic lethality (Kohanski et al., 2007; Meylan et al., 2017; Nandakumar et al., 2014) and validate the fidelity of our white-box machine learning approach.

Interestingly, a second cluster appeared, possessing purine biosynthesis pathways (“superpathway of histidine, purine, and pyrimidine biosynthesis” and “superpathway of purine nucleotides *de novo* biosynthesis II”) with shared directionality between AMP and CIP and opposite directionality for GENT. To our knowledge, purine biosynthesis has not been implicated previously as a mechanism of antibiotic lethality from any biochemical

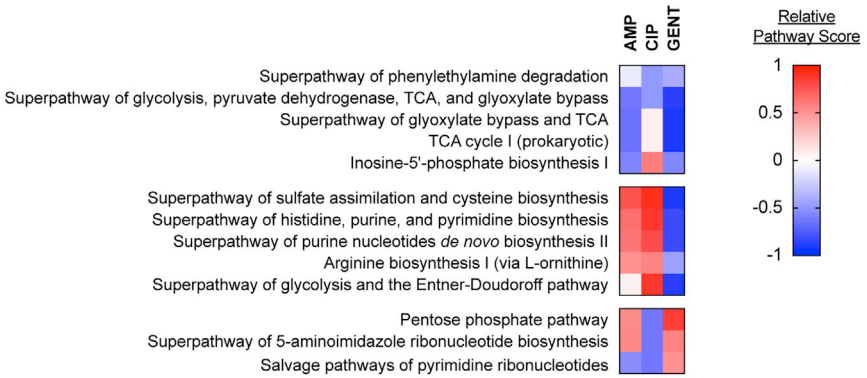

Figure 3. White-Box Machine Learning Reveals Known and New Antibiotic Mechanisms of Action

Shown are pathway scores for metabolic pathways identified by white-box machine learning. Identified pathways include several central carbon metabolism and nucleotide biosynthesis pathways, and these cluster into three groups based on pathway score. Central metabolism pathways primarily exhibit a similar pathway directionality for AMP, CIP, and GENT, whereas purine biosynthesis pathways exhibit a different pathway score directionality for GENT than from AMP or CIP. Pathway scores were computed for each antibiotic by log-transforming the average regression coefficient for all non-zero reactions annotated in a given pathway.

or chemogenomic screen. To better understand these differences in pathway directionality, we examined the regression coefficients for each reaction and computed a reaction score by log-transforming their magnitudes. These analyses identified early steps in the purine biosynthesis pathway as being primarily responsible for the predicted differences for AMP and CIP from GENT (Figure S1). These findings illustrate how white-box machine learning can reveal new mechanisms of action with high biochemical specificity.

Purine Biosynthesis Activity Participates in Antibiotic Lethality

Motivated by the above model-guided machine learning predictions, we sought to test whether perturbations to purine biosynthesis would alter antibiotic lethality. From the predictions, we hypothesized that genetic deletion of enzymes involved in purine metabolism would exert differential effects on AMP and CIP lethality compared with GENT lethality. Indeed, *E. coli* mutants deficient for *purD* (glycinamide ribonucleotide synthetase), *purE* (N^5-carboxyaminoimidazole ribonucleotide mutase), *purK* (5-(carboxyamino)imidazole ribonucleotide synthase), or *purM* (phosphoribosylformylglycinamide cyclo-ligase), early steps in purine biosynthesis (Figure 4A), exhibited significant decreases in AMP and CIP lethality but increased GENT lethality compared with the wild type (Figure 4B). Similarly, biochemical inhibition of purine biosynthesis with 6-mercaptopurine, a *PurF* (amidophosphoribosyltransferase) inhibitor, decreases AMP and CIP lethality but increases GENT lethality (Figure 4C). These effects appear to be specific to purine metabolism because genetic deletion of enzymes involved in pyrimidine biosynthesis did not elicit significant differences in AMP, CIP, or GENT lethality (Figure S2A).

Cells deficient for *glyA* (serine hydroxymethyltransferase), which participates in producing tetrahydrofolate co-factors through the folate cycle, also exhibited decreased AMP and CIP lethality but increased GENT lethality (Figure 4D). Similar phenotypes were observed under combination treatment with trimethoprim, a potent biochemical inhibitor of *FolA* (dihydrofolate reductase) (Figure S2B), consistent with previous findings (Lobritz et al., 2015; Ocampo et al., 2014; Paisley and Washington, 1978).

We further hypothesized that stimulation of purine biosynthesis would elicit opposite effects on antibiotic lethality than inhibition by these genetic and biochemical perturbations. Indeed, biochemical supplementation with the purine biosynthesis substrates phosphoribosyl pyrophosphate (prpp) and glutamine (gln) (Figure 4A, blue) led to increased AMP and CIP lethality and decreased GENT lethality (Figure 4E). Collectively, these data support the model-driven hypothesis that purine biosynthesis participates in antibiotic lethality and demonstrate how model-guided machine learning can provide reductive, hypothesis-driven mechanistic insights into drug efficacy.

Adenine Limitation Contributes to Antibiotic Lethality

Bactericidal antibiotics significantly alter bacterial metabolism as part of their lethality, increasing the abundance of intracellular central carbon metabolites and disrupting the nucleotide pool (Belenky et al., 2015; Nandakumar et al., 2014; Zampieri et al., 2017). Nucleotide pool disruptions include rapid depletion of free intracellular adenine, guanine, and cytosine and marked accumulation of intracellular uracil (Figure S3). Additionally, nucleotide biosynthesis pathways auto-regulate, with internal feedback inhibition driven biochemically by their nucleotide end products (Figure 5A; Lehninger et al., 2013). Based on the predictions from our white-box machine learning approach and the above observations, we hypothesized that purine supplementation would rescue antibiotic-induced purine depletion and, consequently, decrease the demand for purine biosynthesis, reducing antibiotic lethality. Of note, supplementation with adenine (Figure 5B, red), but not guanine, decreased antibiotic lethality in wild-type cells; these results suggest that adenine limitation rather than guanine limitation drives purine biosynthesis activity under antibiotic stress. We also hypothesized that pyrimidine supplementation would inhibit pyrimidine biosynthesis and promote purine biosynthesis activity via prpp accumulation and, consequently, increase antibiotic lethality. Indeed, supplementation with uracil or cytosine potentiated antibiotic lethality (Figure 5C, blue). Collectively, these data support the hypothesis that purine biosynthesis participates in antibiotic lethality and suggest that antibiotic-induced purine biosynthesis is driven by adenine limitation.

Adenine Supplementation Reduces ATP Demand and Central Carbon Metabolism Activity

Purine biosynthesis is energetically expensive, costing eight ATP molecules to synthesize one adenine molecule from one glucose

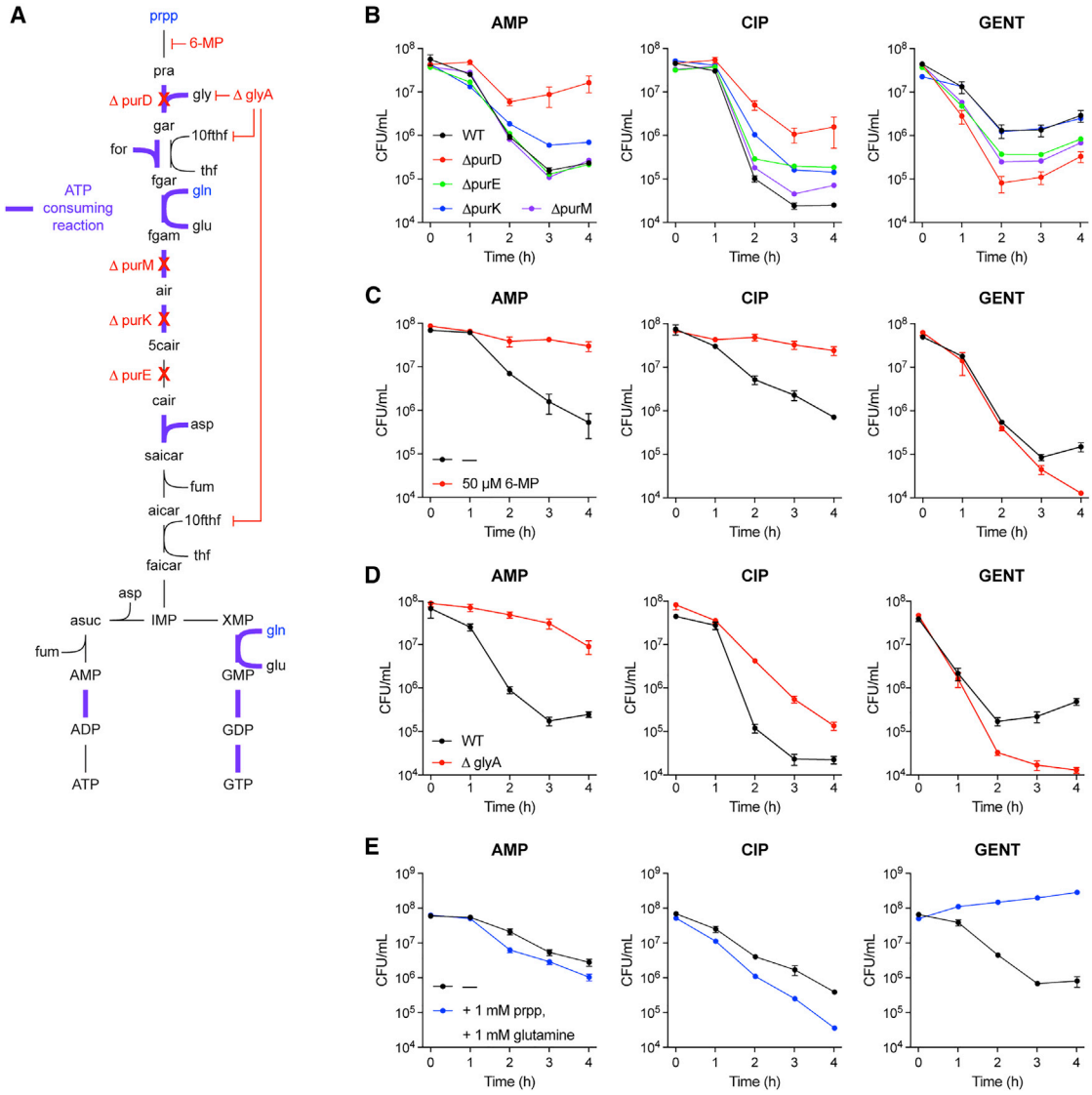

Figure 4. Purine Biosynthesis Participates in Antibiotic Lethality

(A) Purine biosynthesis pathway. Purine biosynthesis begins with phosphoribosyl pyrophosphate (prpp) and contains several ATP-consuming steps (purple).

(B) Antibiotic lethality in purine biosynthesis deletion mutants. Genetic inhibition of purine biosynthesis by *purD* (glycinamide ribonucleotide synthetase), *purE* (N^5-carboxyaminoimidazole ribonucleotide mutase), *purK* (5-(carboxyamino)imidazole ribonucleotide synthase), or *purM* (phosphoribosylformylglycinamide cyclo-ligase) deletion decreases AMP and CIP lethality but increases GENT lethality.

(C) Antibiotic lethality following biochemical inhibition of purine biosynthesis. Biochemical inhibition of *PurF* (amidophosphoribosyltransferase) by 6-mercaptopurine (6-MP) decreases AMP and CIP lethality but increases GENT lethality.

(D) Antibiotic lethality in a *glyA* (serine hydroxymethyltransferase) deletion mutant. Genetic inhibition of glycine (gly) and N^{10}-formyl-tetrahydrofolate (10fthf) by *glyA* deletion decreases AMP and CIP lethality but increases GENT lethality.

(E) Antibiotic lethality following enhanced purine biosynthesis. Substrate-level stimulation of purine biosynthesis with prpp and glutamine (gln) supplementation increases AMP and CIP lethality but decreases GENT lethality.

Data are represented as mean ± SEM from n ≥ 3 independent biological replicates.

molecule (Lehninger et al., 2013). To better understand the mechanistic basis for the observed differences in antibiotic lethality under adenine or uracil supplementation, we examined the simulated metabolic network states corresponding to these perturbations (Table S5). Model simulations predicted that adenine supplementation would decrease purine biosynthesis and, consequently, decrease ATP utilization by nucleotide synthesis and salvage reactions whereas uracil supplementation would not (Figure 6A). Model simulations also predicted that, as a result of these changes, overall flux through central carbon metabolism pathways would decrease, reducing the activity of enzymes involved in cellular respiration and oxidative

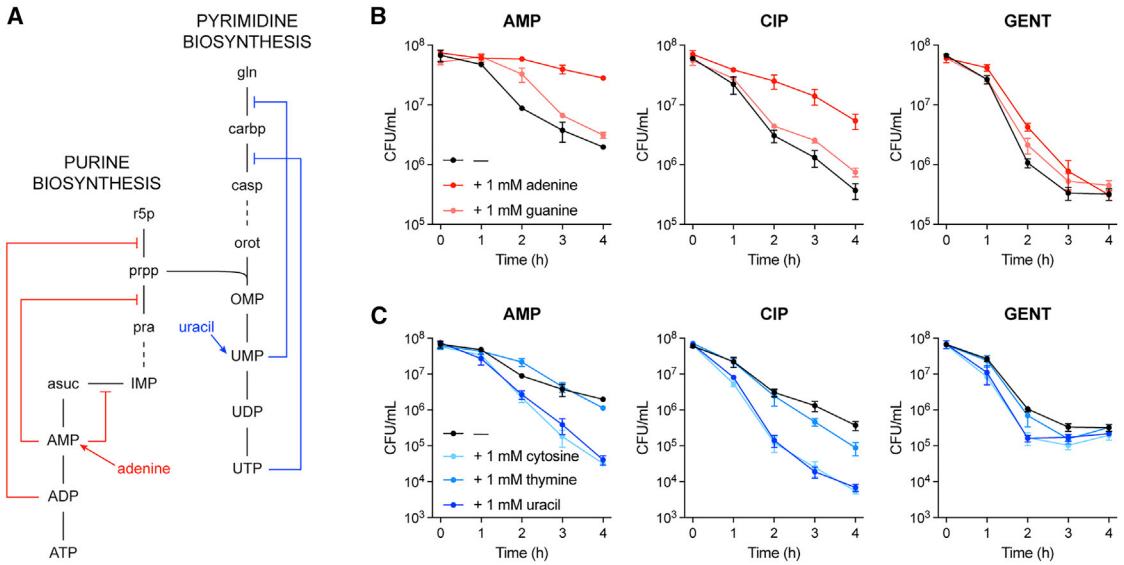

Figure 5. Adenine Limitation Contributes to Antibiotic Lethality

(A) Feedback inhibition in the purine and pyrimidine biosynthesis pathways. Purine and pyrimidine biosynthesis auto-regulate through internal feedback inhibition by nucleotide end products.

(B) Antibiotic lethality following purine supplementation. Adenine supplementation (red) decreases AMP, CIP, and GENT lethality.

(C) Antibiotic lethality following pyrimidine supplementation. Uracil supplementation (dark blue) increases AMP, CIP, and GENT lethality.

Data are represented as mean ± SEM from n = 3 independent biological replicates.

phosphorylation, such as succinate dehydrogenase (Figure S4). These modeling results are consistent with previous observations that glycolytic flux is controlled by ATP demand (Koebmann et al., 2002).

We tested these metabolic modeling predictions by quantifying the intracellular concentrations of central carbon metabolism and energy currency metabolites from *E. coli* cells grown in MOPS minimal medium and supplemented with either adenine or uracil (Figure 6B; Table S8). Under these conditions, cell growth did not significantly change in the first hour of supplementation (Figure S5A), but intracellular adenine nucleotides did accumulate under exogenous adenine addition (Figure S5B). Consistent with model predictions that adenine supplementation would inhibit succinate dehydrogenase activity, intracellular succinate increased, whereas intracellular fumarate decreased (Figure 6C). Model simulations additionally predicted that ATP synthesis would decrease under adenine supplementation (Figure 6D, left). Consistent with this, we observed a modest decrease in the adenylate energy charge (Figure 6D, right), an index for the energy state of a cell (Chapman and Atkinson, 1977). We also examined the relative changes in intracellular nicotinamide adenine dinucleotides under adenine or uracil supplementation (Figure S5C) and observed a modest decrease in the NADPH:-$NADP^+$ ratio, but not the NADH:NAD^+ ratio, following exogenous adenine addition (Figure 6E). Together, these results support the model predictions that adenine supplementation decreases central carbon metabolism activity (decreased adenylate energy charge) and cell anabolism (decreased NADPH:$NADP^+$ ratio) without significantly changing cell catabolism (unchanged NADH:NAD^+ ratio) (Figure S5D; Andersen and von Meyenburg, 1977; Chapman and Atkinson, 1977).

The metabolic modeling simulations further predicted that decreases in oxidative phosphorylation under adenine supplementation lead to decreases in cellular oxygen consumption (Figure 6F, left). We tested these modeling predictions using a Seahorse XF analyzer and measured changes in the oxygen consumption rate (OCR) following antibiotic treatment with or without adenine or uracil supplementation. Antibiotic treatment with AMP, CIP, or GENT increased the cellular oxygen consumption rate (Figure 6F, black), in contrast to control conditions (Figure S5E), supporting previous observations that cellular respiration is important for antibiotic lethality (Gutierrez et al., 2017; Lobritz et al., 2015). Importantly, adenine supplementation significantly repressed changes in cellular oxygen consumption under antibiotic treatment (Figure 6F, red), consistent with model predictions, whereas uracil enhanced cellular oxygen consumption (Figure 6F, blue). These results directly support the hypothesis that central carbon metabolism activity and cellular respiration are increased under antibiotic stress to satisfy the elevated ATP demand resulting from purine biosynthesis. Collectively, our data and simulations indicate that adenine limitation resulting from antibiotic treatment drives purine biosynthesis, which increases ATP demand, fueling the redox-associated metabolic alterations involved in antibiotic lethality (Dwyer et al., 2014; Figure 7).

DISCUSSION

Recent advances in high-throughput experimental technologies and data science have stimulated considerable interest in the potential for artificial intelligence to transform biological discovery and healthcare (Gil et al., 2014; Topol, 2019; Webb, 2018; Yu

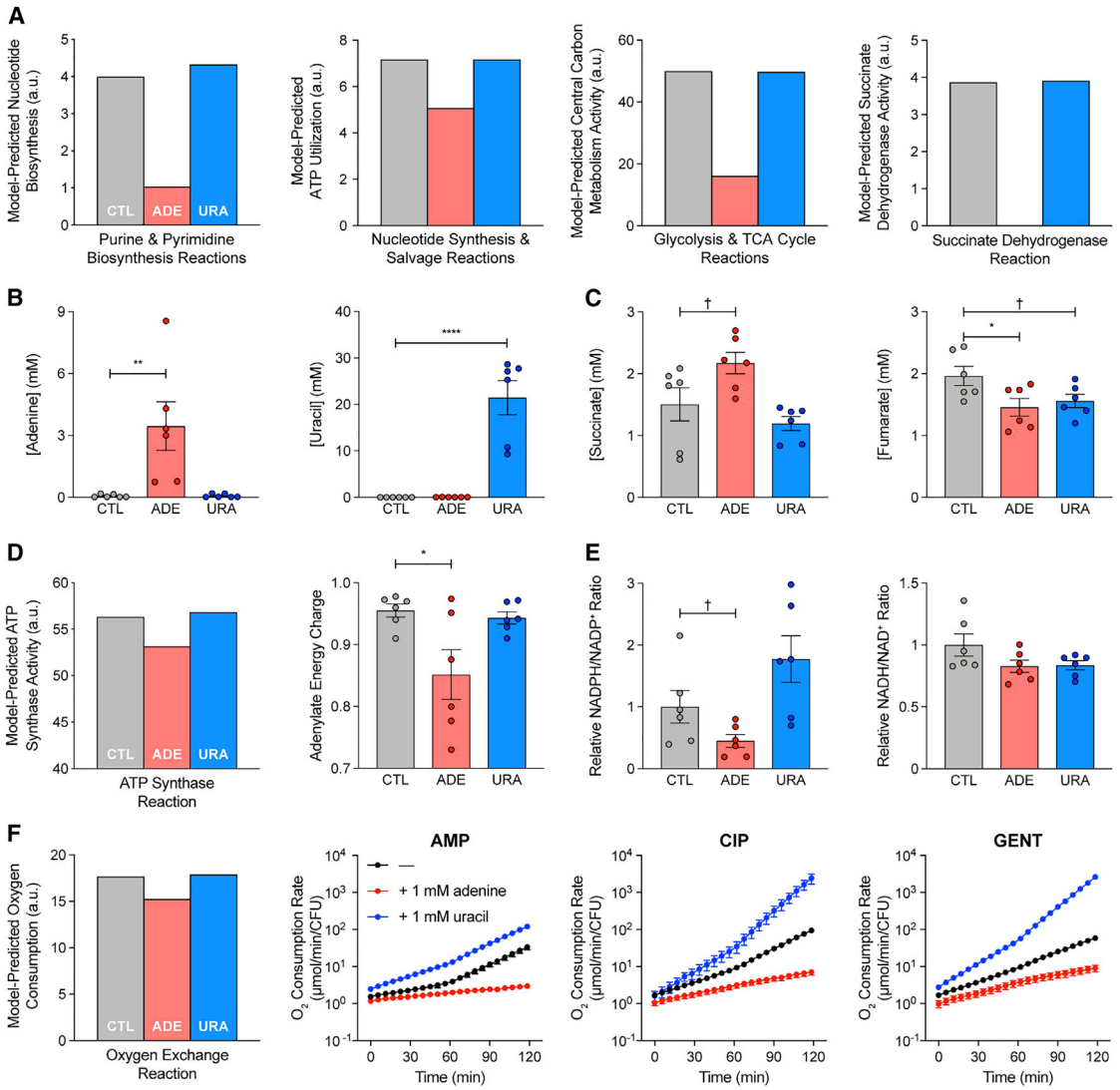

Figure 6. Adenine Supplementation Reduces ATP Demand and Central Carbon Metabolism Activity

(A) Metabolic modeling predictions. Adenine supplementation decreases activity through purine biosynthesis, consequently decreasing ATP utilization by purine biosynthesis, central carbon metabolism, and oxidative phosphorylation (Figure S4) in comparison with the simulated control (CTL). *E. coli* metabolism under adenine (ADE) or uracil (URA) supplementation was simulated by parsimonious flux balance analysis (pFBA) in the iJO1366 metabolic model, with exchange reactions for adenine or uracil opened, respectively. Nucleotide biosynthesis activity was computed by summing fluxes through reactions in the purine and pyrimidine biosynthesis subsystem (left). ATP consumption was summed across all reactions in the purine and pyrimidine biosynthesis and nucleotide salvage pathway subsystems (center left). Central carbon metabolism activity was computed by summing fluxes through reactions in the glycolysis and TCA cycle subsystems (center right). Oxidative phosphorylation is proxied by the succinate dehydrogenase reaction (right); additional oxidative phosphorylation reactions are depicted in Figure S4. All fluxes were normalized by the biomass objective function.

(B) Intracellular adenine or uracil concentrations following adenine or uracil supplementation. Intracellular metabolite concentrations were measured by targeted liquid chromatography-tandem mass spectrometry (LC-MS/MS).

(C) Intracellular succinate or fumarate concentrations following adenine or uracil supplementation. Adenine supplementation increases intracellular succinate and decreases intracellular fumarate, consistent with model predictions for inhibited succinate dehydrogenase activity (A, right).

(D) ATP synthesis following adenine or uracil supplementation. Metabolic modeling simulations predict a decrease in ATP synthesis following adenine supplementation (left), reported by the ATP synthase reaction. Metabolomic measurements of intracellular ATP, ADP, and AMP (Figure S5B) reveal a similar decrease in adenylate energy charge following adenine supplementation (right).

(E) NADPH:$NADP^+$ and NADH:NAD^+ ratios following adenine or uracil supplementation. Metabolomic measurements of intracellular NADPH, $NADP^+$, NADH, and NAD^+ (Figure S5C) reveal modest decreases in the NADPH:$NADP^+$ ratio following adenine supplementation (left), indicating reduced anabolic metabolism. The NADH:NAD^+ ratio is largely unchanged (right), indicating preserved catabolic metabolism.

(F) Cellular respiration following adenine or uracil supplementation during antibiotic treatment. Metabolic modeling simulations predict a decrease in oxygen consumption following adenine supplementation (left), reported by the oxygen exchange reaction. Adenine supplementation (red) reduces respiratory activity,

(legend continued on next page)

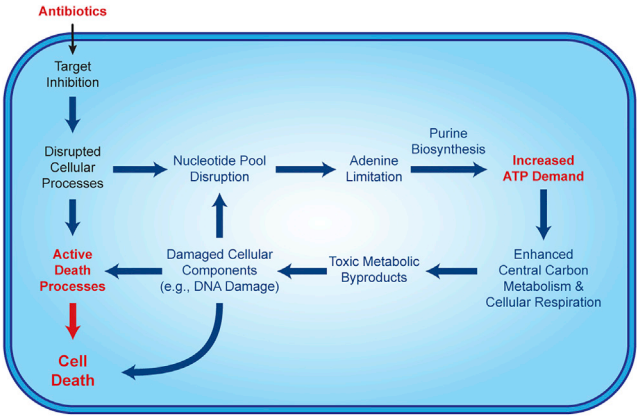

Figure 7. Antibiotic-Induced Adenine Limitation Induces Purine Biosynthesis, Increasing ATP Demand and Driving Central Carbon Metabolism Activity

In addition to the lethal effects of inhibiting their primary targets, bactericidal antibiotics disrupt the nucleotide pool, depleting intracellular purines and inducing adenine limitation. Adenine limitation triggers purine biosynthesis, increasing ATP demand, which drives increased activity through central carbon metabolism and cellular respiration. Toxic metabolic byproducts generated by this increased metabolic activity damage DNA and exacerbate antibiotic-mediated killing. Futile cycles and other stress-induced phenomena may also elevate ATP demand.

et al., 2018a). Important for such pursuits will be the necessary transition from correlation-based machine learning to causality-based "machine reasoning" (Bottou, 2014). Identifying causal mechanisms by modern machine learning approaches is challenging because of the mechanistic inaccessibility of computationally derived black-box associations between perturbations and phenotypes. In this study, we show how biological network models can be utilized to overcome this mechanistic uncertainty and help uncover biological mechanisms (Camacho et al., 2018; Yu et al., 2018b).

Network modeling has long provided a foundation for systems biology (Ideker et al., 2001), and researchers are now beginning to integrate machine learning with retrospective network modeling for improving the fidelity of genotype-to-phenotype predictions (Ma et al., 2018). Such activities demonstrate how hierarchically organized prior knowledge can deconvolve complex biological data; however, these efforts rely on *post hoc* analyses of experimental data and can only perform inductive association of phenotypes with perturbations rather than deductive identification of the causal mechanisms driving phenotypes. Here we present a complementary approach, combining machine learning with prospective network modeling to infer biological mechanisms based on their combined information content.

We demonstrate how this approach can be integrated with biochemical screening and applied to understanding mechanisms underlying antibiotic efficacy. Antibiotics are conventionally understood to work by inhibiting processes involved in bacterial cell replication (Kohanski et al., 2010). However, recent work has shown that processes downstream of target inhibition, including bacterial metabolism, actively participate in antibiotic lethality (Cho et al., 2014; Dwyer et al., 2015; Gruber and Walker, 2018; Zhao and Drlica, 2014). An important knowledge gap has been in understanding the biological mechanisms underlying antibiotic-mediated changes in metabolism. Our results here suggest that altered metabolism resulting from bactericidal antibiotic treatment is driven in part by the increased ATP required to restore homeostasis to a disrupted nucleotide pool (Belenky et al., 2015). It is likely that antibiotic-induced insults to the nucleotide pool are further exacerbated by nucleotide oxidation (Fan et al., 2018; Foti et al., 2012; Gruber and Walker, 2018), resulting in a positive feedback loop of increased nucleotide biosynthesis, elevated central carbon metabolism, and toxic metabolic byproduct generation that is lethally detrimental to the cell (Figure 7). Because nucleotide analogs are commonly used as Food and Drug Administration (FDA)-approved anticancer and antiviral chemotherapeutics, it will be interesting to explore their potential as antimicrobial agents or adjuvants (El Zahed and Brown, 2018; Serpi et al., 2016).

Adenine nucleotides are important mediators of cellular homeostasis (Andersen and von Meyenburg, 1977; Chapman and Atkinson, 1977), universally coupling cellular metabolism, DNA or RNA replication, and other physiological processes. In the context of infection, adenylate metabolites such as ATP, ADP, and adenosine are important components of the damage-associated molecular patterns used by the host to activate the immune system (Cekic and Linden, 2016). We observed previously that adenine metabolites such as AMP accumulate at a site of infection during antibiotic treatment and, consistent with our data here, can inhibit antibiotic lethality (Yang et al., 2017b). Given our results, it is likely that inter-patient differences in the concentrations of extracellular nucleotides contribute to variable antibiotic treatment outcomes for infection (Lee and Collins, 2011). Moreover, our finding that uracil potentiates antibiotic lethality (Figures 5) suggests that pyrimidine nucleotides may potentially be useful as antimicrobial adjuvants.

Evolution has optimized bacteria for efficient resource allocation under unstressed growth (Basan et al., 2015; Hui et al., 2015; Scott et al., 2014), and insults to the ATP pool and other energy currencies are sufficient for stimulating central carbon metabolism (Holm et al., 2010; Koebmann et al., 2002) and sensitizing cells to oxidative stress (Adolfsen and Brynildsen, 2015). Additionally, intracellular ATP and the adenylate energy charge are tightly regulated across the tree of life and robustly maintained across environmental conditions and cellular insults (Chapman and Atkinson, 1977). Under antibiotic stress, increases to ATP demand are likely to arise from multiple sources (Yang et al., 2017a). Consistent with these notions, pharmacological suppression of oxidative phosphorylation (Shetty and Dick, 2018) and metabolic conditions inhibiting intracellular ATP (Shan et al., 2017) protect cells against antibiotics, supporting a critical

whereas uracil (blue) increases respiratory activity. Changes in the oxygen consumption rate following treatment with AMP, CIP, or GENT and adenine or uracil supplementation were measured using the Seahorse extracellular flux analyzer.

Data are represented as mean ± SEM from n = 3 independent biological replicates. Significance is reported as FDR-corrected p values in comparison with the control: †$p \leq 0.1$, *$p \leq 0.05$, **$p \leq 0.01$, ****$p \leq 0.0001$.

role for ATP dynamics in antibiotic-mediated lethality. Additionally, futile cycling in cell wall synthesis and degradation was recently reported to be a component of β-lactam lethality (Cho et al., 2014). Our findings support a new fundamental concept in understanding antibiotic death physiology; namely, that stress-induced changes in ATP utilization and demand, as a homeostatic response, critically drive lethal metabolic alterations. Because antibiotic stress increases the abundance of central carbon metabolism intermediates (Belenky et al., 2015; Nandakumar et al., 2014) and TCA cycle protein expression (Babin et al., 2017), central carbon metabolism is worth exploring as a target for antimicrobial drug discovery (Bald et al., 2017; Murima et al., 2014).

The growing global crisis of antibiotic resistance has created a clear imperative for expanded efforts in antimicrobial drug discovery and investigations into bacterial cellular death physiology (Brown and Wright, 2016). As experimental and computational technologies mature, new techniques and resources are becoming available for studying the biological mechanisms underlying antibiotic responses in complex and dynamic environments (Certain et al., 2017; Dunphy and Papin, 2018; Mack et al., 2018; Yang et al., 2017a). Although the work described here has specifically focused on bacterial metabolism, several other aspects of bacterial physiology are known to be relevant to antibiotic efficacy, including bacterial stress responses, DNA repair mechanisms, and macromolecular processes such as transcription and translation (Dwyer et al., 2015; Gruber and Walker, 2018; Yang et al., 2017a). Investigation into these other physiological systems will require new and different modeling approaches (Carrera and Covert, 2015; Ma et al., 2018; Oberhardt et al., 2013; Yang et al., 2018), curated knowledge bases (Karr et al., 2012; Keseler et al., 2017; Monk et al., 2017), and screening innovations (French et al., 2016, 2018). Integration of such resources with machine learning could advance antibiotic discovery by revealing novel mechanisms that can be targeted with next-generation adjuvants, boosting our existing antibiotic arsenal (Tyers and Wright, 2019).

White-box machine learning can be broadly extended across diverse biological systems and, as demonstrated here, be impactful for revealing drug mechanisms of action for treating human diseases. For instance, cell metabolism is increasingly recognized as being important in cancer pathogenesis (Vander Heiden and DeBerardinis, 2017), and histidine metabolism was recently demonstrated to participate in the efficacy of some cancer therapeutics (Kanarek et al., 2018). Similar to the present work on antibiotics, cancer drugs may be counter-screened against a library of metabolites in human cancer cells and coupled with network simulations using models of human metabolism (Brunk et al., 2018) to discover metabolic mechanisms of action for existing cancer drugs. Insights gained by such an approach may help guide the design of cancer treatment regimens, accounting for a tumor's local metabolic microenvironment and leveraging metabolic perturbations to optimize treatment outcomes.

Moreover, our integrated screening-modeling-learning approach is agnostic to the experimental datasets and network models used to train machine learning models. NIH Common Fund programs such as Library of Integrated Network-Based Cellular Signatures (LINCS) and Big Data to Knowledge are providing increasingly comprehensive measurements of cellular physiology in response to genetic or small-molecule perturbations (Keenan et al., 2018). Our white-box machine learning approach could be extended to such datasets to reveal molecular mechanisms mediating cellular responses to biochemical stimuli. For instance, simulations may be performed on human signaling networks to transform LINCS small-molecule perturbations into signaling network configurations that can be utilized as input data to learn signaling mechanisms of epigenetic regulation from measured chromatin signatures (Litichevskiy et al., 2018). Similarly, prospective network simulations may be performed on gene-regulatory networks to interpret CRISPR screening perturbations (Wang et al., 2014) and reveal transcriptional programs underlying screened phenotypes.

Finally, white-box machine learning will be important for realizing the transformative promises of translational precision medicine activities such as the NIH's All of Us research program. Simulations may be performed on biological networks curated in databases such as BioGRID (Stark et al., 2006) to transform human data from repositories such as the UK Biobank (Bycroft et al., 2018) into gene-regulatory, signaling, or metabolic network states customized for each individual patient in a diverse population. These customized network states may be applied as inputs to machine learning models to identify mechanistically interpretable biomarkers and molecular mechanisms of disease pathogenesis from relevant clinical metadata using classification and regression techniques. Such analyses could be impactful for treating human disease by enabling stratified, personalized treatment strategies based on an individual's gene-regulatory, signaling, or metabolic network state and by providing new targets for drug discovery programs (Yu et al., 2018a). Reaching such endpoints will require continued high-quality characterization of human specimens and curation of human biological networks. However, white-box machine learning will reward such efforts with deep new insights that could enable truly personalized medicine.

STAR★METHODS

Detailed methods are provided in the online version of this paper and include the following:

- KEY RESOURCES TABLE
- CONTACT FOR REAGENT AND RESOURCE SHARING
- EXPERIMENTAL MODEL AND SUBJECT DETAILS
  - Bacterial Strains, Media, Growth Conditions, Reagents
- METHOD DETAILS
  - Metabolite Screen and IC_{50} Determination
  - Gene Knockout Strain Construction
  - Time-Kill Experiments
  - Intracellular Metabolite Quantification
  - Oxygen Consumption Rate Quantification
- QUANTIFICATION AND STATISTICAL ANALYSIS
  - Hierarchical Clustering
  - Metabolite Set Enrichment Analysis
  - Genome-Scale Metabolic Modeling
  - Multitask Elastic Net Regularization

- Hypergeometric Pathway Identification
- Pathway and Reaction Score Computation
- Metabolite Quantification
- Statistical Analysis

SUPPLEMENTAL INFORMATION

Supplemental Information can be found online at https://doi.org/10.1016/j.cell.2019.04.016.

ACKNOWLEDGMENTS

The authors thank Ian Andrews, Sarah Bening, and Charley Gruber from MIT; Eric Brown and Madeline Tong from McMaster University; Eytan Ruppin from the National Cancer Institute; Ahmed Badran, Eachan Johnson, and Keren Yizhak from the Broad Institute; Sylvie Manuse from Northeastern University; and Xilin Zhao from New Jersey Medical School for helpful discussions. This work was supported by grant HDTRA1-15-1-0051 from the Defense Threat Reduction Agency (to J.J.C.), grant K99-GM118907 from the NIH (to J.H.Y.), a National Science Foundation graduate research fellowship 1122374 (to M.A.A.), grant U01-AI124316 from the NIH (to B.O.P.), the Novo Nordisk Foundation (to B.O.P.), grants R01-CA021615 and R35-ES028303 from the NIH (to G.C.W.); grant U19-AI111276 from the NIH (to J.J.C.), and support from the Paul G. Allen Frontiers Group, the Broad Institute at MIT and Harvard, and the Wyss Institute for Biologically Inspired Engineering (to J.J.C). G.C.W. is an American Cancer Society professor.

AUTHOR CONTRIBUTIONS

Conceptualization, J.H.Y.; Methodology, J.H.Y., S.N.W., M.H., D.M., M.A.A., L.S., and A.J.L.; Investigation, J.H.Y., S.N.W., M.H., D.M., M.A.A., L.S., A.J.L., S.S., and A.N.; Formal Analysis, J.H.Y., S.N.W., and D.M.; Visualization, J.H.Y.; Writing, J.H.Y., G.C.W., and J.J.C.; Resources, J.J.C., B.O.P., and J.H.Y.; Funding Acquisition, J.J.C., G.C.W., B.O.P., and J.H.Y.; Supervision, B.O.P, G.C.W., and J.J.C.

DECLARATION OF INTERESTS

J.J.C. is a scientific co-founder and scientific advisory board chair of Enbiotix, an antibiotics startup company.

Received: September 10, 2018
Revised: March 19, 2019
Accepted: April 8, 2019
Published: May 9, 2019

REFERENCES

Adolfsen, K.J., and Brynildsen, M.P. (2015). Futile cycling increases sensitivity toward oxidative stress in Escherichia coli. Metab. Eng. *29*, 26–35.

Allison, K.R., Brynildsen, M.P., and Collins, J.J. (2011). Metabolite-enabled eradication of bacterial persisters by aminoglycosides. Nature *473*, 216–220.

Andersen, K.B., and von Meyenburg, K. (1977). Charges of nicotinamide adenine nucleotides and adenylate energy charge as regulatory parameters of the metabolism in Escherichia coli. J. Biol. Chem. *252*, 4151–4156.

Baba, T., Ara, T., Hasegawa, M., Takai, Y., Okumura, Y., Baba, M., Datsenko, K.A., Tomita, M., Wanner, B.L., and Mori, H. (2006). Construction of Escherichia coli K-12 in-frame, single-gene knockout mutants: the Keio collection. Mol. Syst. Biol. *2*, 2006.0008.

Babin, B.M., Atangcho, L., van Eldijk, M.B., Sweredoski, M.J., Moradian, A., Hess, S., Tolker-Nielsen, T., Newman, D.K., and Tirrell, D.A. (2017). Selective Proteomic Analysis of Antibiotic-Tolerant Cellular Subpopulations in *Pseudomonas aeruginosa* Biofilms. MBio *8*, e01593-17.

Bald, D., Villellas, C., Lu, P., and Koul, A. (2017). Targeting Energy Metabolism in *Mycobacterium tuberculosis*, a New Paradigm in Antimycobacterial Drug Discovery. MBio *8*, 8.

Basan, M., Hui, S., Okano, H., Zhang, Z., Shen, Y., Williamson, J.R., and Hwa, T. (2015). Overflow metabolism in Escherichia coli results from efficient proteome allocation. Nature *528*, 99–104.

Belenky, P., Ye, J.D., Porter, C.B., Cohen, N.R., Lobritz, M.A., Ferrante, T., Jain, S., Korry, B.J., Schwarz, E.G., Walker, G.C., and Collins, J.J. (2015). Bactericidal Antibiotics Induce Toxic Metabolic Perturbations that Lead to Cellular Damage. Cell Rep. *13*, 968–980.

Bochner, B.R. (2009). Global phenotypic characterization of bacteria. FEMS Microbiol. Rev. *33*, 191–205.

Bottou, L. (2014). From machine learning to machine reasoning. Mach. Learn. *94*, 133–149.

Brown, E.D., and Wright, G.D. (2016). Antibacterial drug discovery in the resistance era. Nature *529*, 336–343.

Brunk, E., Sahoo, S., Zielinski, D.C., Altunkaya, A., Dräger, A., Mih, N., Gatto, F., Nilsson, A., Preciat Gonzalez, G.A., Aurich, M.K., et al. (2018). Recon3D enables a three-dimensional view of gene variation in human metabolism. Nat. Biotechnol. *36*, 272–281.

Bycroft, C., Freeman, C., Petkova, D., Band, G., Elliott, L.T., Sharp, K., Motyer, A., Vukcevic, D., Delaneau, O., O'Connell, J., et al. (2018). The UK Biobank resource with deep phenotyping and genomic data. Nature *562*, 203–209.

Camacho, D.M., Collins, K.M., Powers, R.K., Costello, J.C., and Collins, J.J. (2018). Next-Generation Machine Learning for Biological Networks. Cell *173*, 1581–1592.

Carrera, J., and Covert, M.W. (2015). Why Build Whole-Cell Models? Trends Cell Biol. *25*, 719–722.

Caruana, R. (1997). Multitask Learning. Mach. Learn. *28*, 41–75.

Cekic, C., and Linden, J. (2016). Purinergic regulation of the immune system. Nat. Rev. Immunol. *16*, 177–192.

Certain, L.K., Way, J.C., Pezone, M.J., and Collins, J.J. (2017). Using Engineered Bacteria to Characterize Infection Dynamics and Antibiotic Effects In Vivo. Cell Host Microbe *22*, 263–268.e4.

Chapman, A.G., and Atkinson, D.E. (1977). Adenine nucleotide concentrations and turnover rates. Their correlation with biological activity in bacteria and yeast. Adv. Microb. Physiol. *15*, 253–306.

Ching, T., Himmelstein, D.S., Beaulieu-Jones, B.K., Kalinin, A.A., Do, B.T., Way, G.P., Ferrero, E., Agapow, P.M., Zietz, M., Hoffman, M.M., et al. (2018). Opportunities and obstacles for deep learning in biology and medicine. J. R. Soc. Interface *15*, 20170387.

Cho, H., Uehara, T., and Bernhardt, T.G. (2014). Beta-lactam antibiotics induce a lethal malfunctioning of the bacterial cell wall synthesis machinery. Cell *159*, 1300–1311.

Dunphy, L.J., and Papin, J.A. (2018). Biomedical applications of genome-scale metabolic network reconstructions of human pathogens. Curr. Opin. Biotechnol. *51*, 70–79.

Dwyer, D.J., Belenky, P.A., Yang, J.H., MacDonald, I.C., Martell, J.D., Takahashi, N., Chan, C.T., Lobritz, M.A., Braff, D., Schwarz, E.G., et al. (2014). Antibiotics induce redox-related physiological alterations as part of their lethality. Proc. Natl. Acad. Sci. USA *111*, E2100–E2109.

Dwyer, D.J., Collins, J.J., and Walker, G.C. (2015). Unraveling the physiological complexities of antibiotic lethality. Annu. Rev. Pharmacol. Toxicol. *55*, 313–332.

El Zahed, S.S., and Brown, E.D. (2018). Chemical-Chemical Combinations Map Uncharted Interactions in Escherichia coli under Nutrient Stress. iScience *2*, 168–181.

Fan, X.Y., Tang, B.K., Xu, Y.Y., Han, A.X., Shi, K.X., Wu, Y.K., Ye, Y., Wei, M.L., Niu, C., Wong, K.W., et al. (2018). Oxidation of dCTP contributes to antibiotic lethality in stationary-phase mycobacteria. Proc. Natl. Acad. Sci. USA *115*, 2210–2215.

Foti, J.J., Devadoss, B., Winkler, J.A., Collins, J.J., and Walker, G.C. (2012). Oxidation of the guanine nucleotide pool underlies cell death by bactericidal antibiotics. Science *336*, 315–319.

French, S., Mangat, C., Bharat, A., Côté, J.P., Mori, H., and Brown, E.D. (2016). A robust platform for chemical genomics in bacterial systems. Mol. Biol. Cell *27*, 1015–1025.

French, S., Coutts, B.E., and Brown, E.D. (2018). Open-Source High-Throughput Phenomics of Bacterial Promoter-Reporter Strains. Cell Syst. *7*, 339–346.e3.

Gil, Y., Greaves, M., Hendler, J., and Hirsh, H. (2014). Artificial Intelligence. Amplify scientific discovery with artificial intelligence. Science *346*, 171–172.

Gruber, C.C., and Walker, G.C. (2018). Incomplete base excision repair contributes to cell death from antibiotics and other stresses. DNA Repair (Amst.) *71*, 108–117.

Gutierrez, A., Jain, S., Bhargava, P., Hamblin, M., Lobritz, M.A., and Collins, J.J. (2017). Understanding and Sensitizing Density-Dependent Persistence to Quinolone Antibiotics. Mol. Cell *68*, 1147–1154.e3.

Holm, A.K., Blank, L.M., Oldiges, M., Schmid, A., Solem, C., Jensen, P.R., and Vemuri, G.N. (2010). Metabolic and transcriptional response to cofactor perturbations in Escherichia coli. J. Biol. Chem. *285*, 17498–17506.

Honaker, J., King, G., and Blackwell, M. (2011). Amelia II: A Program for Missing Data. J. Stat. Softw. *45*, 1–47.

Hui, S., Silverman, J.M., Chen, S.S., Erickson, D.W., Basan, M., Wang, J., Hwa, T., and Williamson, J.R. (2015). Quantitative proteomic analysis reveals a simple strategy of global resource allocation in bacteria. Mol. Syst. Biol. *11*, 784.

Ideker, T., Galitski, T., and Hood, L. (2001). A new approach to decoding life: systems biology. Annu. Rev. Genomics Hum. Genet. *2*, 343–372.

Kanarek, N., Keys, H.R., Cantor, J.R., Lewis, C.A., Chan, S.H., Kunchok, T., Abu-Remaileh, M., Freinkman, E., Schweitzer, L.D., and Sabatini, D.M. (2018). Histidine catabolism is a major determinant of methotrexate sensitivity. Nature *559*, 632–636.

Karr, J.R., Sanghvi, J.C., Macklin, D.N., Gutschow, M.V., Jacobs, J.M., Bolival, B., Jr., Assad-Garcia, N., Glass, J.I., and Covert, M.W. (2012). A whole-cell computational model predicts phenotype from genotype. Cell *150*, 389–401.

Keenan, A.B., Jenkins, S.L., Jagodnik, K.M., Koplev, S., He, E., Torre, D., Wang, Z., Dohlman, A.B., Silverstein, M.C., Lachmann, A., et al. (2018). The Library of Integrated Network-Based Cellular Signatures NIH Program: System-Level Cataloging of Human Cells Response to Perturbations. Cell Syst. *6*, 13–24.

Keseler, I.M., Mackie, A., Santos-Zavaleta, A., Billington, R., Bonavides-Martínez, C., Caspi, R., Fulcher, C., Gama-Castro, S., Kothari, A., Krummenacker, M., et al. (2017). The EcoCyc database: reflecting new knowledge about Escherichia coli K-12. Nucleic Acids Res. *45* (D1), D543–D550.

Koebmann, B.J., Westerhoff, H.V., Snoep, J.L., Nilsson, D., and Jensen, P.R. (2002). The glycolytic flux in Escherichia coli is controlled by the demand for ATP. J. Bacteriol. *184*, 3909–3916.

Kohanski, M.A., Dwyer, D.J., Hayete, B., Lawrence, C.A., and Collins, J.J. (2007). A common mechanism of cellular death induced by bactericidal antibiotics. Cell *130*, 797–810.

Kohanski, M.A., Dwyer, D.J., and Collins, J.J. (2010). How antibiotics kill bacteria: from targets to networks. Nat. Rev. Microbiol. *8*, 423–435.

Lee, H.H., and Collins, J.J. (2011). Microbial environments confound antibiotic efficacy. Nat. Chem. Biol. *8*, 6–9.

Lehninger, A.L., Nelson, D.L., and Cox, M.M. (2013). Lehninger principles of biochemistry, Sixth Edition (New York: W.H. Freeman).

Lewis, N.E., Hixson, K.K., Conrad, T.M., Lerman, J.A., Charusanti, P., Polpitiya, A.D., Adkins, J.N., Schramm, G., Purvine, S.O., Lopez-Ferrer, D., et al. (2010). Omic data from evolved E. coli are consistent with computed optimal growth from genome-scale models. Mol. Syst. Biol. *6*, 390.

Litichevskiy, L., Peckner, R., Abelin, J.G., Asiedu, J.K., Creech, A.L., Davis, J.F., Davison, D., Dunning, C.M., Egertson, J.D., Egri, S., et al. (2018). A Library of Phosphoproteomic and Chromatin Signatures for Characterizing Cellular Responses to Drug Perturbations. Cell Syst. *6*, 424–443.e7.

Lobritz, M.A., Belenky, P., Porter, C.B., Gutierrez, A., Yang, J.H., Schwarz, E.G., Dwyer, D.J., Khalil, A.S., and Collins, J.J. (2015). Antibiotic efficacy is linked to bacterial cellular respiration. Proc. Natl. Acad. Sci. USA *112*, 8173–8180.

Lu, R., Lee, G.C., Shultz, M., Dardick, C., Jung, K., Phetsom, J., Jia, Y., Rice, R.H., Goldberg, Z., Schnable, P.S., et al. (2008). Assessing probe-specific dye and slide biases in two-color microarray data. BMC Bioinformatics *9*, 314.

Ma, J., Yu, M.K., Fong, S., Ono, K., Sage, E., Demchak, B., Sharan, R., and Ideker, T. (2018). Using deep learning to model the hierarchical structure and function of a cell. Nat. Methods *15*, 290–298.

Machado, D., and Herrgård, M. (2014). Systematic evaluation of methods for integration of transcriptomic data into constraint-based models of metabolism. PLoS Comput. Biol. *10*, e1003580.

Mack, S.G., Turner, R.L., and Dwyer, D.J. (2018). Achieving a Predictive Understanding of Antimicrobial Stress Physiology through Systems Biology. Trends Microbiol. *26*, 296–312.

McCloskey, D., Gangoiti, J.A., King, Z.A., Naviaux, R.K., Barshop, B.A., Palsson, B.O., and Feist, A.M. (2014). A model-driven quantitative metabolomics analysis of aerobic and anaerobic metabolism in E. coli K-12 MG1655 that is biochemically and thermodynamically consistent. Biotechnol. Bioeng. *111*, 803–815.

McCloskey, D., Xu, J., Schrübbers, L., Christensen, H.B., and Herrgård, M.J. (2018). RapidRIP quantifies the intracellular metabolome of 7 industrial strains of E. coli. Metab. Eng. *47*, 383–392.

Megchelenbrink, W., Huynen, M., and Marchiori, E. (2014). optGpSampler: an improved tool for uniformly sampling the solution-space of genome-scale metabolic networks. PLoS ONE *9*, e86587.

Meylan, S., Porter, C.B.M., Yang, J.H., Belenky, P., Gutierrez, A., Lobritz, M.A., Park, J., Kim, S.H., Moskowitz, S.M., and Collins, J.J. (2017). Carbon Sources Tune Antibiotic Susceptibility in Pseudomonas aeruginosa via Tricarboxylic Acid Cycle Control. Cell Chem. Biol. *24*, 195–206.

Milo, R., and Phillips, R. (2016). Cell biology by the numbers (New York, NY: Garland Science, Taylor & Francis Group).

Monk, J.M., Lloyd, C.J., Brunk, E., Mih, N., Sastry, A., King, Z., Takeuchi, R., Nomura, W., Zhang, Z., Mori, H., et al. (2017). iML1515, a knowledgebase that computes Escherichia coli traits. Nat. Biotechnol. *35*, 904–908.

Murima, P., McKinney, J.D., and Pethe, K. (2014). Targeting bacterial central metabolism for drug development. Chem. Biol. *21*, 1423–1432.

Nandakumar, M., Nathan, C., and Rhee, K.Y. (2014). Isocitrate lyase mediates broad antibiotic tolerance in Mycobacterium tuberculosis. Nat. Commun. *5*, 4306.

Neidhardt, F.C., Bloch, P.L., and Smith, D.F. (1974). Culture medium for enterobacteria. J. Bacteriol. *119*, 736–747.

Oberhardt, M.A., Yizhak, K., and Ruppin, E. (2013). Metabolically re-modeling the drug pipeline. Curr. Opin. Pharmacol. *13*, 778–785.

Ocampo, P.S., Lázár, V., Papp, B., Arnoldini, M., Abel zur Wiesch, P., Busa-Fekete, R., Fekete, G., Pál, C., Ackermann, M., and Bonhoeffer, S. (2014). Antagonism between bacteriostatic and bactericidal antibiotics is prevalent. Antimicrob. Agents Chemother. *58*, 4573–4582.

Orth, J.D., Conrad, T.M., Na, J., Lerman, J.A., Nam, H., Feist, A.M., and Palsson, B.O. (2011). A comprehensive genome-scale reconstruction of Escherichia coli metabolism–2011. Mol. Syst. Biol. *7*, 535.

Paisley, J.W., and Washington, J.A., 2nd. (1978). Synergistic activity of gentamicin with trimethoprim or sulfamethoxazole-trimethoprim against Escherichia coli and Klebsiella pneumoniae. Antimicrob. Agents Chemother. *14*, 656–658.

Pedregosa, F., Varoquaux, G., Gramfort, A., Michel, V., Thirion, B., Grisel, O., Blondel, M., Prettenhofer, P., Weiss, R., Dubourg, V., et al. (2011). Scikit-learn: Machine Learning in Python. J. Mach. Learn. Res. *12*, 2825–2830.

Roses, A.D. (2008). Pharmacogenetics in drug discovery and development: a translational perspective. Nat. Rev. Drug Discov. *7*, 807–817.

Schellenberger, J., Que, R., Fleming, R.M., Thiele, I., Orth, J.D., Feist, A.M., Zielinski, D.C., Bordbar, A., Lewis, N.E., Rahmanian, S., et al. (2011). Quantitative prediction of cellular metabolism with constraint-based models: the COBRA Toolbox v2.0. Nat. Protoc. *6*, 1290–1307.

Scott, M., Klumpp, S., Mateescu, E.M., and Hwa, T. (2014). Emergence of robust growth laws from optimal regulation of ribosome synthesis. Mol. Syst. Biol. *10*, 747.

Serpi, M., Ferrari, V., and Pertusati, F. (2016). Nucleoside Derived Antibiotics to Fight Microbial Drug Resistance: New Utilities for an Established Class of Drugs? J. Med. Chem. *59*, 10343–10382.

Shan, Y., Brown Gandt, A., Rowe, S.E., Deisinger, J.P., Conlon, B.P., and Lewis, K. (2017). ATP-Dependent Persister Formation in Escherichia coli. MBio *8*, e02267-16.

Shetty, A., and Dick, T. (2018). Mycobacterial Cell Wall Synthesis Inhibitors Cause Lethal ATP Burst. Front. Microbiol. *9*, 1898.

Stark, C., Breitkreutz, B.J., Reguly, T., Boucher, L., Breitkreutz, A., and Tyers, M. (2006). BioGRID: a general repository for interaction datasets. Nucleic Acids Res. *34*, D535–D539.

Topol, E.J. (2019). High-performance medicine: the convergence of human and artificial intelligence. Nat. Med. *25*, 44–56.

Tyers, M., and Wright, G.D. (2019). Drug combinations: a strategy to extend the life of antibiotics in the 21st century. Nat. Rev. Microbiol. *17*, 141–155.

Vander Heiden, M.G., and DeBerardinis, R.J. (2017). Understanding the Intersections between Metabolism and Cancer Biology. Cell *168*, 657–669.

Wainberg, M., Merico, D., Delong, A., and Frey, B.J. (2018). Deep learning in biomedicine. Nat. Biotechnol. *36*, 829–838.

Wang, T., Wei, J.J., Sabatini, D.M., and Lander, E.S. (2014). Genetic screens in human cells using the CRISPR-Cas9 system. Science *343*, 80–84.

Webb, S. (2018). Deep learning for biology. Nature *554*, 555–557.

Xie, L., Draizen, E.J., and Bourne, P.E. (2017). Harnessing Big Data for Systems Pharmacology. Annu. Rev. Pharmacol. Toxicol. *57*, 245–262.

Yang, J.H., Bening, S.C., and Collins, J.J. (2017a). Antibiotic efficacy-context matters. Curr. Opin. Microbiol. *39*, 73–80.

Yang, J.H., Bhargava, P., McCloskey, D., Mao, N., Palsson, B.O., and Collins, J.J. (2017b). Antibiotic-Induced Changes to the Host Metabolic Environment Inhibit Drug Efficacy and Alter Immune Function. Cell Host Microbe *22*, 757–765.e3.

Yang, L., Yurkovich, J.T., King, Z.A., and Palsson, B.O. (2018). Modeling the multi-scale mechanisms of macromolecular resource allocation. Curr. Opin. Microbiol. *45*, 8–15.

Yu, K.-H., Beam, A.L., and Kohane, I.S. (2018a). Artificial intelligence in healthcare. Nat. Biomed. Eng. *2*, 719–731.

Yu, M.K., Ma, J., Fisher, J., Kreisberg, J.F., Raphael, B.J., and Ideker, T. (2018b). Visible Machine Learning for Biomedicine. Cell *173*, 1562–1565.

Yuan, H., Paskov, I., Paskov, H., González, A.J., and Leslie, C.S. (2016). Multitask learning improves prediction of cancer drug sensitivity. Sci. Rep. *6*, 31619.

Zampieri, M., Zimmermann, M., Claassen, M., and Sauer, U. (2017). Nontargeted Metabolomics Reveals the Multilevel Response to Antibiotic Perturbations. Cell Rep. *19*, 1214–1228.

Zhao, X., and Drlica, K. (2014). Reactive oxygen species and the bacterial response to lethal stress. Curr. Opin. Microbiol. *21*, 1–6.

Zou, H., and Hastie, T. (2005). Regularization and variable selection via the elastic net. J. R. Stat. Soc. Series B Stat. Methodol. *67*, 301–320.

STAR★METHODS

KEY RESOURCES TABLE

REAGENT or RESOURCE	SOURCE	IDENTIFIER
Bacterial and Virus Strains		
Escherichia coli K-12 MG1655	ATCC	ATCC 700926
Chemicals, Peptides, and Recombinant Proteins		
6-Mercaptopurine	Sigma-Aldrich	Cat# 852678-1G-A; CAS: 6112-76-1
^{13}C-Glucose	Cambridge Isotope Laboratories	Cat# CLM-1396-1; CAS: 110187-42-3
Adenine	Sigma-Aldrich	Cat# A8626-5G; CAS: 73-24-5
Ampicillin	Sigma-Aldrich	Cat# A9518-5G; CAS: 69-52-3
Ciprofloxacin	Sigma-Aldrich	Cat# 17850-25G-F; CAS: 85721-33-1
Cytosine	Sigma-Aldrich	Cat# C3506-1G; CAS: 71-30-7
Gentamicin	Sigma-Aldrich	Cat# G1914-5G; CAS: 1405-41-0
Glutamine	Sigma-Aldrich	Cat# G8540-25G; CAS: 56-85-9
Guanine	Sigma-Aldrich	Cat# G11950-10G; CAS: 73-40-5
MOPS EZ Rich Defined Medium Kit	Teknova	Cat# M2105
MOPS Minimal Media Kit	Teknova	Cat# M2106
Phenotype Microarray 1 MicroPlate	Biolog (Bochner, 2009)	Cat# 12111
Phenotype Microarray 2 MicroPlate	Biolog (Bochner, 2009)	Cat# 12112
Phenotype Microarray 3 MicroPlate	Biolog (Bochner, 2009)	Cat# 12121
Phenotype Microarray 4 MicroPlate	Biolog (Bochner, 2009)	Cat# 12131
Phosphoribosyl pyrophosphate	Sigma-Aldrich	Cat# P8296-100MG; CAS: 108321-05-7
Thymine	Sigma-Aldrich	Cat# T0376-100G; CAS: 65-71-4
Trimethoprim	Sigma-Aldrich	Cat# T7883-5G; CAS: 738-70-5
Uracil	Sigma-Aldrich	Cat# U0750-100G; CAS: 66-22-8
Oligonucleotides		
See Table S9	This paper	N/A
Software and Algorithms		
MATLAB 2018a	Mathworks	https://www.mathworks.com/
COBRA Toolbox v. 2.0	(Schellenberger et al., 2011)	https://opencobra.github.io/cobratoolbox/
Gurobi Optimizer v. 6.0.4	Gurobi Optimization	http://www.gurobi.com/
optGpSampler	(Megchelenbrink et al., 2014)	http://cs.ru.nl/~wmegchel/optGpSampler/
Spyder IDE v. 3.3.0	Spyder Project Contributors	https://www.spyder-ide.org/
scikit-learn v. 0.17.0	(Pedregosa et al., 2011)	https://scikit-learn.org/
Ecocyc v. 22.0	(Keseler et al., 2017)	https://ecocyc.org/
Prism v. 8.0.2	GraphPad	https://www.graphpad.com/
AB SCIEX MultiQuant v. 3.0.1	SCIEX	https://sciex.com/products/software/multiquant-software
Amelia II v. 1.7.4	(Honaker et al., 2011)	https://cran.r-project.org/web/packages/Amelia/index.html
LMGene v. 3.3	(Lu et al., 2008)	http://www.bioconductor.org/packages/release/bioc/html/LMGene.html

CONTACT FOR REAGENT AND RESOURCE SHARING

Further information and requests for resources and reagents should be directed to and will be fulfilled by the Lead Contact, James J. Collins (jimjc@mit.edu).

EXPERIMENTAL MODEL AND SUBJECT DETAILS

Bacterial Strains, Media, Growth Conditions, Reagents

Escherichia coli strain K-12 MG1655 (ATCC 700926) was used for all experiments in this study. For metabolite supplementation experiments, cells were cultured in MOPS minimal medium with 0.2% glucose (Teknova; Hollister, CA). For experiments involving gene deletions, cells were cultured in MOPS EZ Rich defined medium (Teknova). For all experiments, cells were grown at 37°C either on a rotating shaker at 300 rpm in baffled flasks or 14 mL test tubes or on a rotating shaker at 900 rpm in Biolog 96-well phenotype microarrays (Bochner, 2009) (Biolog; Hayward, CA). All experiments were performed with $n \geq 3$ biological replicates from independent overnight cultures. Uniformly labeled ^{13}C glucose was purchased from Cambridge Isotope Laboratories, Inc. (Tewksbury, MA). LC-MS reagents were purchased from Honeywell Burdick & Jackson® (Muskegon, MI) and Sigma-Aldrich (St. Louis, MO).

METHOD DETAILS

Metabolite Screen and IC_{50} Determination

An overnight culture of *E. coli* cells in MOPS minimal medium was diluted 1:500 and grown to mid-exponential phase at 37°C with 300 rpm shaking in 2 L baffled flasks. 13 mL cultures were then back-diluted to OD_{600} = 0.1 and dispensed into 14 mL test tubes containing 100x concentrated AMP, CIP or GENT over the following concentration gradients: for AMP, 10 mg/mL, 1 mg/mL and 1.5-fold dilutions from 20 – 0.35 μg/mL; for CIP, 10 μg/mL, 1 μg/mL and 1.5-fold dilutions from 100 – 0.4 ng/mL; for GENT, 10 μg/mL, 1 μg/mL and 1.5-fold dilutions from 200 – 2.6 ng/mL. 100 μL from each antibiotic-treated subculture was dispensed into each well of a Biolog PM 1-4 compound plate. Plates were sealed with breathable membranes and incubated in a 37°C shaking incubator with 900 rpm shaking. After 4 h incubation, OD_{600} was measured on a SpectraMax M5 Microplate Reader (Molecular Devices; San Jose, CA). IC_{50}s were estimated from each set of $n \geq 3$ independent biological replicates by fitting logistic functions to each set of OD_{600} measurements for each well in MATLAB (Mathworks; Natick, MA). In the case of CIP, some metabolite conditions exhibited a biphasic dose-response. For those conditions, a logistic function was fit to only the phase at the lower concentration.

Gene Knockout Strain Construction

E. coli Δ*glyA*, Δ*purD*, Δ*purE*, Δ*purK*, Δ*purM*, Δ*pyrC* and Δ*pyrE* gene deletion mutants were constructed by P1 phage transduction using the Keio collection (Baba et al., 2006), as previously described (Gutierrez et al., 2017). Briefly, P1 phage lysates corresponding to each gene deletion were produced by incubating overnight cultures of Keio donor strains with P1 phage. For each gene deletion, an overnight culture of *E. coli* MG1655 was pelleted and resuspended in a 10 mM $MgCl_2$ and 5 mM $CaCl_2$ salt solution in a 15 mL test tube, and then incubated with the corresponding P1 phage at 37°C for 30 min. Media containing 1 M sodium citrate was added to each tube and incubated at 37°C for an additional 60 min in a 300 rpm shaking incubator. Cells were pelleted, resuspended on fresh media, and then plated on kanamycin-selective agar plates containing 5 mM sodium citrate and incubated overnight at 37°C. Colonies were selected from each plate and their kanamycin-resistance cassettes cured by transducing pCP20 plasmid with electroporation, inducing recombination by overnight growth at 43°C, and then screening resulting colonies for genomic recombination and plasmid loss on kanamycin- and ampicillin-selective agar plates. Overnight cultures of each knockout strain were checked for accuracy by PCR amplification and gel electrophoresis with custom oligonucleotides (Table S9).

Time-Kill Experiments

Time-kill experiments were performed as previously described (Dwyer et al., 2014). An overnight culture of *E. coli* cells in MOPS minimal medium was diluted 1:500 and grown to mid-exponential phase at 37°C with 300 rpm shaking in 125 mL baffled flasks. 1 mL cultures were then back-diluted to OD_{600} = 0.1, dispensed into 14 mL test tubes and treated with AMP, CIP or GENT, with biochemical supplementation where indicated. For all metabolite supplementation experiments in minimal media, time-kill experiments were performed using 4 μg/mL AMP, 16 ng/mL CIP or 48 ng/mL GENT. For all gene knockout experiments in rich media, time-kill experiments were performed using 4 μg/mL AMP, 16 ng/mL CIP or 96 ng/mL GENT. Hourly samples were collected and serially diluted in PBS for colony enumeration 24 h later.

Intracellular Metabolite Quantification

Intracellular metabolites quantified on an AB SCIEX Qtrap® 5500 mass spectrometer (AB SCIEX; Framingham, MA), as previously described (McCloskey et al., 2018), and processed using in house scripts. An overnight culture of *E. coli* cells in MOPS minimal medium was diluted 1:500 and grown to mid-exponential phase at 37°C with 300 rpm shaking in 1 L baffled flasks. 25 mL cultures were then back-diluted to OD_{600} = 0.1, dispensed into 250 mL baffled flasks and treated with either 1 mM adenine, 1 mM uracil or a non-supplemented control. Samples were collected 1 hr after supplementation, and aliquots with biomass equivalents to 10 mL of cell culture at OD_{600} = 0.1 were subjected to metabolite extraction using a 40:40:20 mixture of acetonitrile, methanol and LC-MS grade water. Uniformly labeled ^{13}C-standards were generated by growing *E. coli* in uniformly labeled Glucose M9 minimal media in aerated shake flasks, as previously described (McCloskey et al., 2014). Calibration mixes of standards were split across several mixes, aliquoted, and lyophilized to dryness. All samples and calibrators were equally spiked with the same internal standards. Samples were quantified using isotope-dependent mass spectrometry. Calibration curves were run before and after all biological

and analytical replicates. Consistency of quantification between calibration curves was checked by running a Quality Control sample composed of all biological replicates. Values reported are derived from the average of the biological triplicates, analyzed in duplicate (n = 6).

Oxygen Consumption Rate Quantification

Bacterial respiratory activity was quantified using the Seahorse XF^{e}96 Extracellular Flux Analyzer (Seahorse Bioscience; North Billerica, MA), as previously described (Dwyer et al., 2014; Lobritz et al., 2015). XF Cell Culture Microplates were pre-coated with 100 ng/mL poly-D-lysine. An overnight culture of *E. coli* cells in MOPS minimal medium was diluted 1:500 and grown to mid-exponential phase at 37°C with 300 rpm shaking in 125 mL baffled flasks. Cells were back-diluted to OD_{600} = 0.01 and 90 μL diluted cells were dispensed to each well of the coated XF Microplates. Microplates were centrifuged for 10 min at 4,000 rpm and an additional 90 μL fresh media with or without 1 mM adenine or uracil was added to each well. Antibiotics were added to injection ports and measurements taken at 5 min intervals with 2.5 min measurements cycles and 2.5 min mixing.

QUANTIFICATION AND STATISTICAL ANALYSIS

Hierarchical Clustering

Hierarchical clustering for the measured antibiotic IC_{50}s and identified pathways was performed in MATLAB using the standardized euclidean distance metric.

Metabolite Set Enrichment Analysis

Metabolite Set Enrichment Analysis was performed in Ecocyc (v. 22.0) (Keseler et al., 2017). A SmartTables was created comprised of metabolites eliciting a $\geq$ 2-fold change in IC_{50} for at least one antibiotic (Table S4). Pathways were identified using the ''Enrichment'' analysis type. The Fisher Exact test was performed for each enrichment analysis with false discovery rate (FDR) correction by the Benjamini-Hochberg method.

Genome-Scale Metabolic Modeling

Metabolic simulations were performed using the COBRA Toolbox v. 2.0 (Schellenberger et al., 2011) in MATLAB and Gurobi Optimizer v. 6.0.4 (Gurobi Optimization; Beaverton, OR). Reversible reactions in the iJO1366 *E. coli* model (Orth et al., 2011) were replaced with pairs of forward and backward reactions. In order to simulate growth in MOPS minimal medium, reaction bounds from the exchange reactions corresponding to each metabolite present in MOPS minimal medium were set to a value of '1,000', to permit uptake. Reaction bounds for oxygen exchange, glucose exchange and cobalamin exchange were as set to values of '18.5′, '10' and '0.1', respectively, as previously described (Orth et al., 2011). For each metabolite screening condition, additional exchange reactions were added to represent supplementation with each metabolite on the Biolog phenotype microarray plates (Table S1), with reaction bounds set to '1,000' to permit uptake. Parsimonious flux balance analysis (Lewis et al., 2010) was performed on each metabolite condition-specific model 10,000 times with sampling by optGpSampler (Megchelenbrink et al., 2014). For each reaction in the condition-specific models, the mean flux across all 10,000 samples was computed and used to represent flux in each condition.

Multitask Elastic Net Regularization

Metabolic reactions for each antibiotic were selected using a two-stage multitask elastic net regularization (Yuan et al., 2016; Zou and Hastie, 2005) in the open-source Spyder IDE v. 3.3.0 (Spyder Project Contributors) Python environment. First, IC_{50}s from each screening condition were normalized by their on-plate controls and log_2-transformed. Multitask elastic net was jointly performed on the transformed antibiotic IC_{50}s and the simulated metabolic states using the MultitaskElasticNetCV function in the scikit-learn toolbox v. 0.17.0 (Pedregosa et al., 2011) with 50-fold cross-validation, 1e4 max iterations and tolerance of 1e-6. Second, for each antibiotic, the standard deviation of elastic net coefficients was computed. Reactions whose coefficients possessed magnitude less than half the standard deviation were filtered and removed. Exchange and transport reactions were excluded from this analysis.

Hypergeometric Pathway Identification

Pathways mechanisms were identified by performing hypergeometric statistical testing on metabolic pathways curated in Ecocyc (v. 22.0) (Keseler et al., 2017). For each antibiotic, reactions selected by multitask elastic net regularization were converted to their Ecocyc counterparts and hypergeometric p values were computed for each pathway-reaction set in Spyder. For each antibiotic-pathway combination, FDR statistics were estimated using the Benjamini-Hochberg method. Pathways that exhibited $p \leq 0.05$ and $q \leq 0.05$ for at least one antibiotic were selected.

Pathway and Reaction Score Computation

For each antibiotic, log_2-transformed IC_{50}s were regressed on the reactions selected by multitask elastic net by linear squares using scikit-learn in Spyder. For each pathway, pathway scores were computed by first computing the average of the non-zero regression coefficients for all reactions in each pathway. The magnitudes for these pathway scores were then log_{10}-transformed and normalized

by the largest magnitude of all pathway scores. Reaction scores were computed by taking the $\log_{10}$-transformation of each regression coefficient for each antibiotic. The magnitudes of these reaction scores were then normalized by the largest magnitude of all reaction scores.

Metabolite Quantification

Metabolite concentrations were estimated from LC-MS/MS peak heights using previously generated calibration curves. Metabolites found to have a quantifiable variability (RSD $\geq$ 50%) in the Quality Control samples or possessing individual components with a RSD $\geq$ 80% were excluded from analysis. Metabolites in blanks with a concentration greater than 80% of that found in the biological samples were similarly excluded. Missing values were imputed by bootstrapping using the R package Amelia II (v. 1.7.4, 1,000 imputations) (Honaker et al., 2011). Remaining missing values were approximated as one-half the lower limit of quantification for the metabolite normalized to the biomass of the sample. Intracellular metabolite concentrations were calculated based on an estimated cell density of $7 \cdot 10^7$ CFU/mL at OD_{600} = 0.1 (Figure 5) and an estimated cell volume of 1.3 fL for non-stressed exponential phase *E. coli* cells (Milo and Phillips, 2016).

Statistical Analysis

Statistical significance testing was performed in Prism v8.0.2 (GraphPad; San Diego, CA). One-way ANOVA was performed on intracellular ATP measurements. Reported p values reflect false-discovery correction by the Holm-Šídák multiple comparisons test, with comparisons only between adenine or uracil supplementation with control. Although ANOVA is generally robust against lack of normality in the data, statistical tests were not specifically performed to determine if all of the assumptions of ANOVA had been met.

Cell

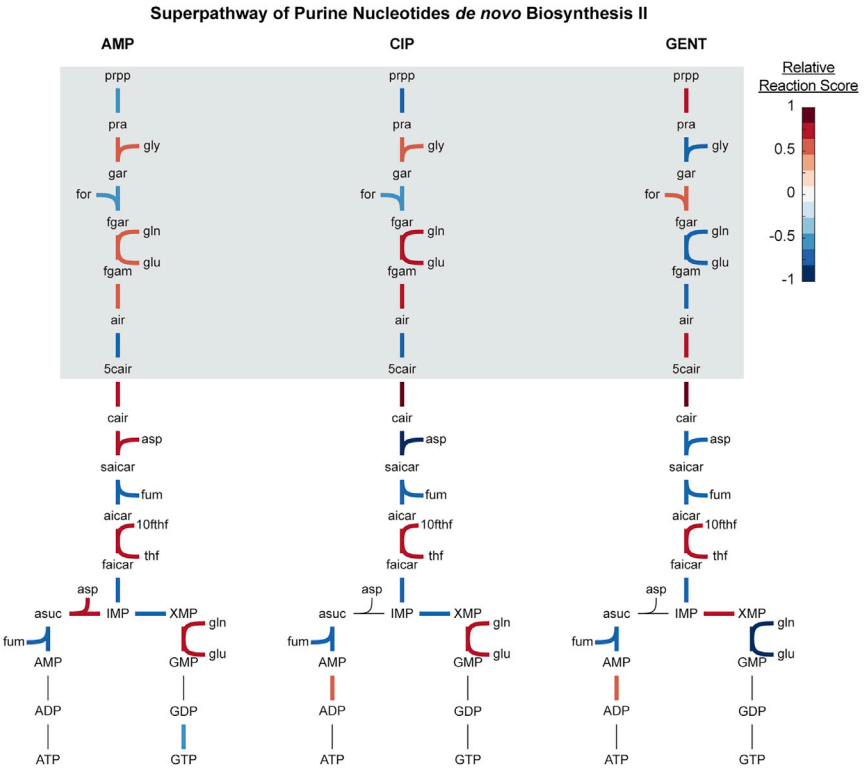

Figure S1. Antibiotic Reaction Scores for Purine Biosynthesis, Related to Figures 3 and 4

Differences in purine biosynthesis pathway scores for ampicillin (AMP) and ciprofloxacin (CIP) from gentamicin (GENT) are primarily explained by early reactions in the purine biosynthesis pathway (gray box).

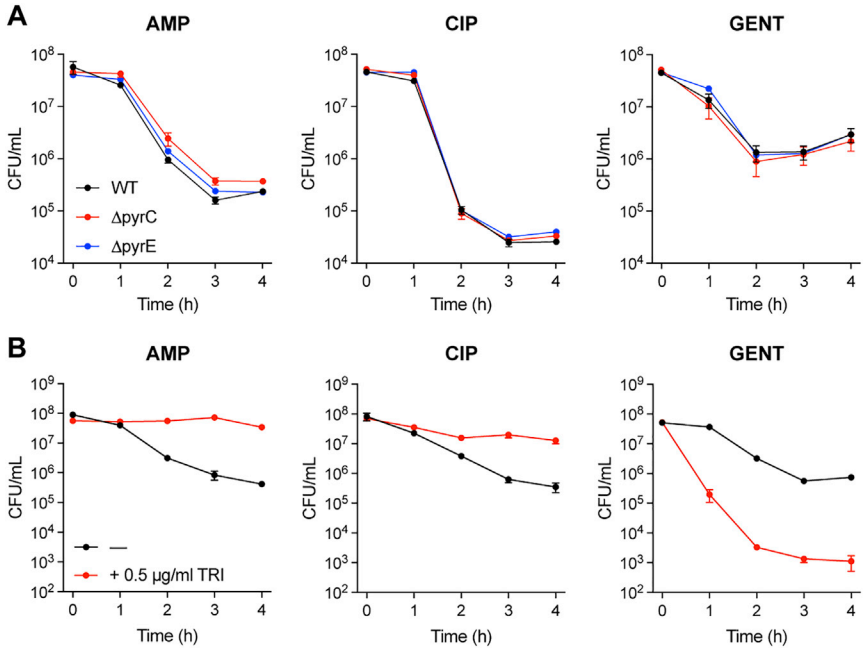

Figure S2. Purine Biosynthesis Participates in Antibiotic Lethality, Related to Figure 4

(A) Antibiotic lethality in pyrimidine biosynthesis deletion mutants. Genetic inhibition of pyrimidine biosynthesis by pyrC (dihydroorotase) or pyrE (orotate phosphoribosyltransferase) deletion does not significantly change ampicillin (AMP), ciprofloxacin (CIP) or gentamicin (GENT) lethality.

(B) Biochemical disruption of the folate cycle by trimethoprim (TRI) decreases AMP and CIP lethality, but increases GENT lethality.

Data are represented as mean ± SEM from n = 3 independent biological replicates.

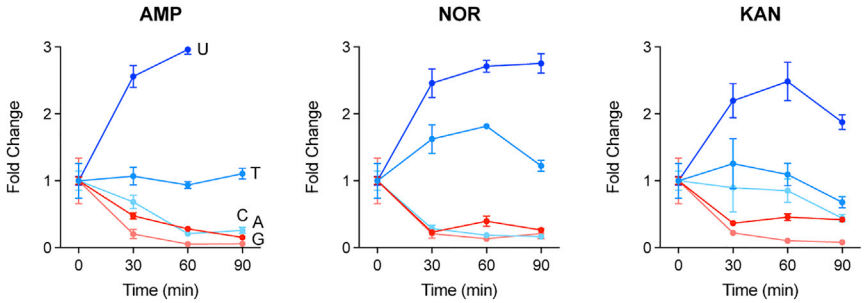

Figure S3. Antibiotic Stress Rapidly Disrupts Intracellular Nucleotide Pools, Related to Figure 5

Purine nucleic acid bases (A: adenine, G: guanine) are depleted (red), while pyrimidine nucleic acid bases (C: cytosine, T: thymine, U: uracil) accumulate (blue) in *E. coli* cells treated with ampicillin (AMP), norfloxacin (NOR) or kanamycin (KAN). Data reanalyzed from Belenky et al., 2015. Data are represented as mean ± SEM from n = 3 independent biological replicates.

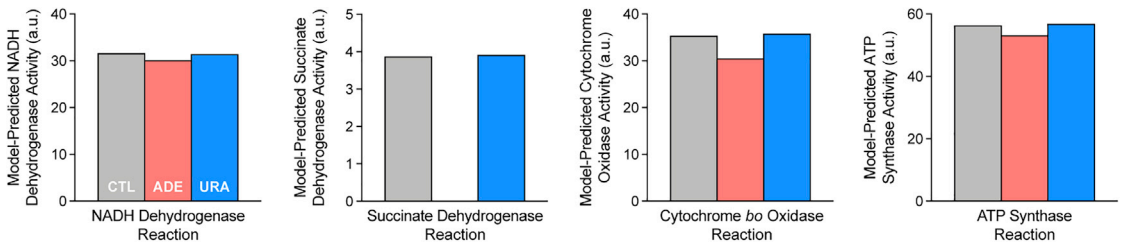

Figure S4. Model Simulations Predict Exogenous Adenine Supplementation Decreases Oxidative Phosphorylation, Related to Figure 6

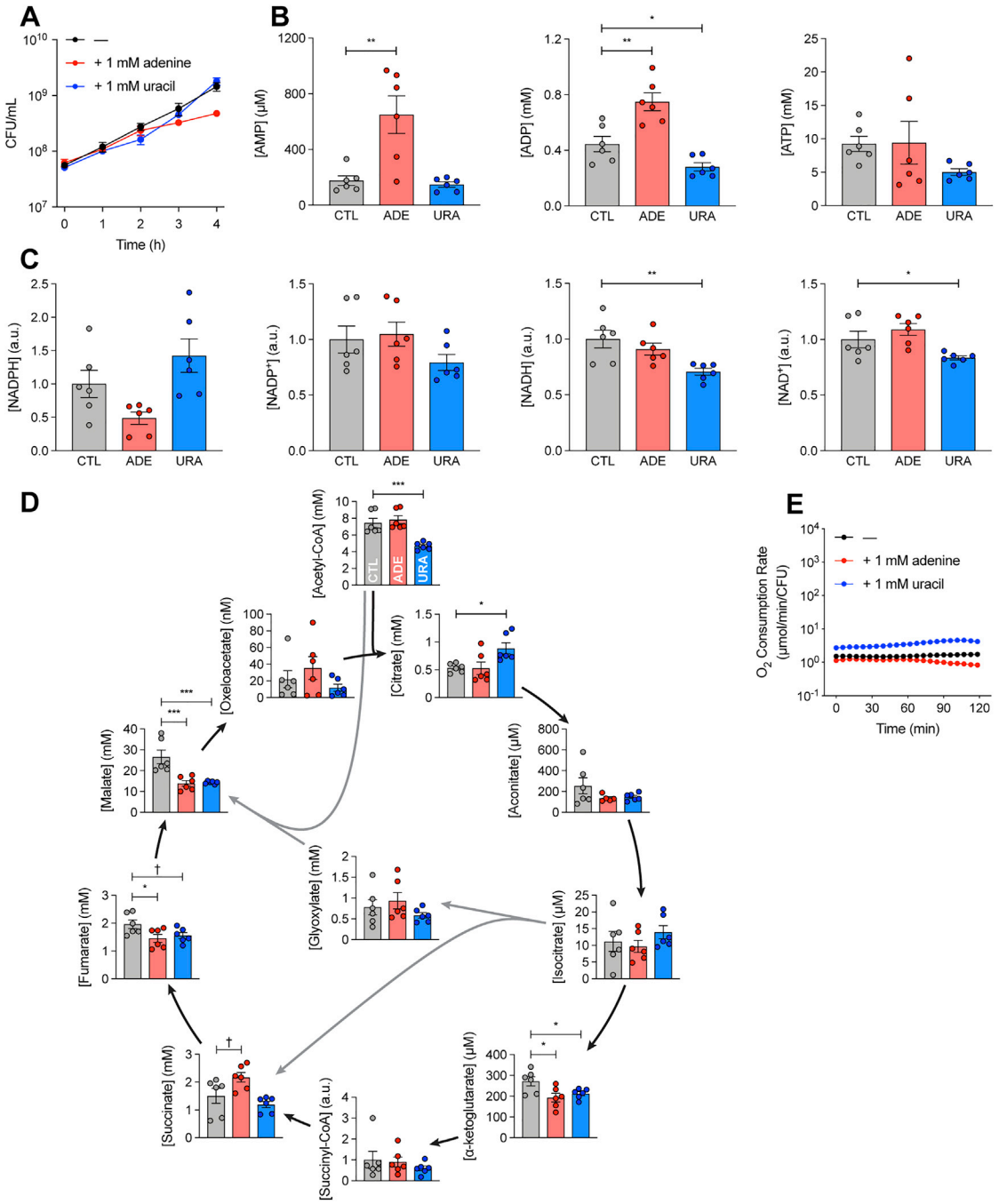

Figure S5. Adenine or Uracil Supplementation Alters Energy Currencies and Central Carbon Metabolism, Related to Figure 6

(A) Exogenous adenine (red) or uracil (blue) supplementation does not significantly alter unstressed growth in MOPS minimal medium.

(B) Intracellular AMP, ADP and ATP concentrations following adenine (ADE) or uracil (URA) supplementation.

(C) Relative intracellular NADPH, $NADP^+$, NADH and NAD^+ concentrations following adenine or uracil supplementation.

(D) Intracellular tricarboxylic acid cycle metabolite concentrations following adenine or uracil supplementation.

(E) Cellular respiration following adenine or uracil supplementation in the absence of antibiotic treatment.

Data are represented as mean ± SEM from n ≥ 3 independent biological replicates. Significance reported as FDR-corrected p values in comparison with control: †: $p \leq 0.1$, *$p \leq 0.05$, **$p \leq 0.01$, ***$p \leq 0.001$.